# Comparative analysis of gene expression in virulent and attenuated strains of infectious bronchitis virus at sub-codon resolution

Adam M. Dinan[1], Sarah Keep[2], Erica Bickerton[2], Paul Britton[2], Andrew E. Firth[1] and Ian Brierley[1†]

[1]Division of Virology, Department of Pathology, University of Cambridge, Tennis Court Road, Cambridge, CB2 1QP, U.K. [2]The Pirbright Institute, Woking, Surrey, GU24 0NF, U.K.

Running Title: Ribosome profiling of coronavirus IBV infection.

[†]Corresponding author: IB: Tel: +44 1223 336914, Fax: +44 1223 336926

Electronic Mail: ib103@cam.ac.uk

Keywords: avian coronavirus, ribosome profiling, RNA virus, RNASeq, translation, differential gene expression

## ABSTRACT

Infectious bronchitis virus (IBV) is a member of the genus *Gammacoronavirus* and the causative agent of avian infectious bronchitis. IBV has a single-stranded, positive-sense RNA genome ~27 kb in length and, like all coronaviruses, produces a set of sub-genomic messenger RNAs (sgmRNAs) synthesised via the viral polymerase. Here, we used RNA sequencing (RNASeq) and ribosome profiling (RiboSeq) to delineate gene expression in the IBV M41-CK and Beau-CK strains at sub-codon resolution. Quantification of reads flanking the programmed ribosomal frameshifting (PRF) signal at the genomic RNA ORF1a/ORF1b junction revealed that PRF in IBV is highly efficient (33–40%), consistent with *in vitro* measurements. Triplet phasing of the profiling data allowed precise determination of reading frames and revealed the translation of two intergenic genes (4b and 4c on sgmRNA4), which are widely conserved across IBV isolates. RNASeq revealed two novel transcription junction sites in the attenuated Beau-CK strain, one of which would generate a sgmRNA encoding a ribosomally occupied ORF in the viral 3' untranslated region (dORF). Within IBV transcripts, the nucleocapsid (N) protein was unexpectedly found to be inefficiently translated, despite being an abundant structural component of mature IBV virions. Finally, we demonstrate that the host cell response to IBV occurs primarily at the level of transcription, with a global up-regulation of immune-related mRNA transcripts following infection, and comparatively modest changes in the translation efficiencies of host genes.


## IMPORTANCE

IBV is a major avian pathogen and presents a substantial economic burden to the poultry industry. Improved vaccination strategies are urgently needed to curb the global spread of this pathogen, and the development of suitable vaccine candidates will be aided by an improved understanding of IBV

molecular biology. Our high-resolution data have enabled a precise study of transcription and translation in both pathogenic and attenuated forms of IBV, and expand our understanding of gammacoronaviral gene expression. We demonstrate that gene expression shows considerable intra-species variation, with single nucleotide polymorphisms associated with altered production of sgmRNA transcripts, and our RiboSeq data sets enabled us to uncover novel ribosomally occupied ORFs in both strains. We also identify numerous cellular genes and gene networks that are differentially expressed during virus infection, giving insights into the host cell reponse to IBV infection.

## INTRODUCTION

Avian infectious bronchitis virus (IBV) is a member of the genus *Gammacoronavirus* (order *Nidovirales*) and a pathogen of the domestic fowl (Cavanagh, 2005). IBV infects primarily the epithelial cells of upper and lower respiratory tract tissues, though infections can also spread to the alimentary canal, as well as to the kidneys, testes and oviduct (Cavanagh, 2007). The monopartite, polycistronic genomic RNA (gRNA) of IBV is approximately 28 kb in length, and – like those of other coronaviruses – it is 5′-methyl-capped and 3′-polyadenylated (Gorbalenya et al., 2006). Two large open reading frames (ORFs) – ORF1a and ORF1b – are situated within the 5′-proximal two-thirds of the genome. Translation of the former yields a *ca.* 3,950-aa polyprotein (pp1a); whereas translation of the latter requires −1 programmed ribosomal frameshifting (PRF) (Brierley et al., 1987; 1989) giving rise to a *ca.* 6,630-aa polyprotein (pp1ab). These polyproteins are cleaved to yield the components of the membrane-bound replication-transcription complex (RTC) (Liu et al., 1997; Brockway et al., 2003; Sawicki et al., 2007). A feature of coronavirus replication is the synthesis of a nested, 3′-coterminal set of subgenomic mRNAs (sgmRNAs) encoding the viral structural and accessory proteins. The 5′ end of each sgmRNA comprises a 56-nt sequence derived from the 5’ end of the genome, the so-called leader sequence (Brown et al., 1986; Sawicki and Sawicki, 1995). Incorporation of the leader occurs as a result of "polymerase hopping" – or discontinuous transcription – during negative-strand synthesis. When the RTC encounters specific “body transcription regulatory sequences” (TRS-Bs), the nascent negative strand can re-pair with a closely homologous leader TRS (TRS-L) at the 3′ end of the leader, after which the viral polymerase completes negative-strand synthesis using the leader as template (**Fig. 1A;** diamond symbols) (Brown et al., 1986; Sawicki and Sawicki, 1995, 1998; Pasternak et al., 2001; Zuniga et al., 2004; Sola et al., 2005; Sawicki et al., 2007). Subsequently, the RTC synthesises positive-strand copies of the negative-strand genomic and sgmRNAs.

Amongst the best-characterised strains of IBV are those belonging to the Massachusetts serotype, which includes the virulent Massachusetts 41 (M41; Van Roekel et al., 1951) isolate and the laboratory-attenuated Beaudette variant (Beaudette and Hudson, 1937). Whilst M41 is restricted to growth in primary chicken cells, Beaudette is capable of replicating in both avian and non-avian cell lines; including Vero (African green monkey kidney-derived) and baby hamster kidney (BHK) cells (Cunningham et al., 1972; Otsuki et al., 1979; Alonso-Caplan et al., 1984; Casais et al., 2003). Polymorphisms in the spike (S) glycoprotein subunit 2 (S2), which spans the viral membrane, have been shown to be responsible for this variation in host cell tropism (Bickerton et al., 2018). Moreover, the S protein of M41 – but not that of Beaudette – elicits an immunoprotective response *in vivo*; although recombinant transfer of the protein from the former to the latter does not restore pathogenicity (Hodgson et al., 1984). The extent to which these strains diverge in terms of virus gene expression, or in terms of host cell gene expression in response to infection, has not been investigated in detail.

The advent of high-throughput sequencing techniques offers a means to monitor viral gene expression at unprecedented resolution (Ingolia et al., 2009; Stern-Ginossar, 2015; Irigoyen et al., 2016; 2018; Stewart et al., 2018). Here, we performed deep sequencing of ribosome-protected fragments (RPFs) – known as RiboSeq – in tandem with whole transcriptome sequencing (RNASeq), on total RNA extracts from primary chicken kidney (CK) cells infected with Beaudette and M41 strains of IBV.

## RESULTS

### RiboSeq and RNASeq Data Quality

RiboSeq and RNASeq libraries were prepared from two biological repeats each of Beau-CK-infected, M41-CK-infected, and mock-infected cells. An average of 1,156,819 RPFs and 1,727,024 RNASeq reads were mapped to viral gRNA in the virus-infected RiboSeq libraries (**Supp. Table S1**). The RNASeq read coverage in the library derived from the second biological repeat of M41-CK-infected cells was lower than that of other libraries due to technical losses. However, 106,741 reads were mapped to the forward strand of the viral gRNA in this case – corresponding to a coverage of approximately 3.8-fold – and these reads were generally evenly distributed along the gRNA; hence, the sequencing depth in this replicate was deemed sufficient for further analysis. The vast majority of RPFs mapping to viral and host protein-coding regions were between 27 and 29 nt in length (**Supp. Fig. S1**), consistent with the size of the RNA fragment protected by translating eukaryotic ribosomes from digestion by RNase I (Wolin and Walter, 1988). The length distributions of RNASeq reads were much broader, in line with the size of the gel slice excised for sequencing of fragmented RNA. RPF length was strongly related to the RPF phase relative to the reading frame of the associated coding region: 27-nt RPFs were primarily in the +1 phase; whereas 28- and 29-nt RPFs were primarily in the 0 phase (**Supp. Fig. S2**). As expected, RNASeq reads were far more evenly split over the three phases, with a slight bias towards phase 0 (**Supp. Fig. S3**), which may reflect codon usage bias – such as a preference for the use of RNY codons (Jukes, 1996; Fuchs et al., 2015; Irigoyen et al., 2016) – compounded with adaptor-ligation bias during library preparation. A meta analysis of host mRNA coding regions showed that the depth of coverage of RiboSeq 5′ read ends increased substantially 12 nt upstream of the AUG (initiation) codon for RPFs in phase 0 (generally 28- and 29-nt RPFs), and 11-nt upstream of the AUG codon for RPFs in phase +1 (generally 27-nt RPFs) (**Supp. Figs. S4 and S5**). This indicates that the ribosomal P-site is situated at an offset of 11 and 12 nt from the 5′ ends of RPFs for 27-nt and 28-/29-nt reads, respectively (Ingolia et al., 2011). Peaks in RNASeq 5′-read end coverage were seen at the A of initiation (AUG)

127 codons and at the middle nucleotide of termination (UNN) codons, respectively (**Supp. Figs. S6**
128 **and S7**), and are considered an artefact of ligation bias.

129

130 **Fig. 1** illustrates the RiboSeq (red) and RNASeq (green) read coverage of the Beaudette **(panel A)**
131 and M41 **(panel B)** genomes. In both cases, the density of RPFs was considerably higher towards
132 the 3′ ends of the gRNA, consistent with production of the 3′ co-terminal nested set of sgmRNAs.
133 In contrast, RiboSeq coverage of the ORF1a and ORF1b coding sequences was relatively low;
134 reflecting the fact that a substantial proportion of newly synthesised gRNA (but not sgmRNA)
135 transcripts are likely to be destined for packaging rather than translation (Kuo and Masters, 2013).
136 On average, negative-sense RNASeq reads were present at 0.28% of the level of positive-sense
137 reads on average, indicating a ratio of positive:negative stranded RNA of ~350:1 at 24 h p.i., a ratio
138 similar to that seen in ribosome profiling studies of the betacoronavirus mouse hepatitis virus
139 (MHV) (Irigoyen et al., 2016). Negative-sense RPFs, which may represent contamination from
140 ribonucleoprotein complexes (Irigoyen et al., 2016), were observed but at low abundance (0.03% of
141 the level of positive-sense RPFs).

142

143 **Virus transcription: sequence divergence associated with IBV strain-specific TRS usage**

144 The density of RNASeq reads mapping to a given sgmRNA represents the cumulative sum of reads
145 derived from the gRNA and those derived from the overlapping portions of other subgenomic
146 transcripts (**Fig. 1**). Therefore, to estimate the abundance of individual sgmRNAs, two independent
147 approaches were used. First, we “decumulated” the raw RNASeq read densities mapping to inter-
148 TRS regions, by subtracting the density of the 5′-adjacent inter-TRS region in each case (Irigoyen et
149 al., 2016). Secondly, the abundances of chimeric RNASeq reads spanning TRS junctions were

quantified, by identifying unmapped reads containing an 11-nt sequence derived from the leader region, 5′-adjacent to the TRS-L (UAGAUUUUUAA, nt 46 – 56 in Beaudette; UAGAUUUCCAA, nt 46 – 56 in M41), and including at least 16 nt 3′ of this query. Chimeric reads were assigned to specific genomic loci based on the sequences 3′ of the TRS in each case (**Supp. Table S2; Fig. 2A**). Overall, the chimeric read abundances for sgmRNAs were significantly correlated with the corresponding decumulated RNASeq densities ($P < 0.01$ in both cases) (**Supp. Fig. S8**). The sequence logos in **Fig. 2B** and **Fig. 2C** illustrate the diversity of nucleotides found at TRS-B sites identified in this study (including the novel sites discussed below) in Beaudette and M41, respectively. The core region of similarity to the TRS-L motif (CUUAACAA) is typically flanked by a 3′ adenine (A) or uracil (U) residue, and a preference for A/U residues is also seen immediately upstream of the core sequence. These flanking residues may facilitate template switching by lowering the free energy of anti-TRS-B/TRS-B duplex disassociation, since the TRS-L is also located in an AU-rich region (Sola et al., 2005).

Notably, the A nucleotides at positions four and seven of the core motif are the only invariant residues. In both Beaudette and M41, the TRS-B sequences associated with the S gene contain G residues at the third positions (CUGAACAA); in contrast to the TRS-L, which has a U at this position (CUUAACAA) (**Supp. Table S2**). Chimeric reads assigned to this gene were found to contain either a U or a G residue at position three (denoted “S [U3]” and “S [G3]”, respectively, in **Fig. 2A; Supp. Table S2**); with a G being more common in M41 (7.5% of reads compared with 5.8%, on average) and a U being more common in Beaudette (2.1% of reads compared with 1.5%, on average) (**Supp. Table S2**). These data indicate that the exact position at which discontinuous transcription occurs within a given TRS is subject to some variation, with either the TRS-L or the TRS-B templating the third residue. Similarly, the TRS-B for the 3a/3b/E genes diverges at the third position between Beaudette (CUGAACAA; nt 23825 – 23832) and M41 (CUUAACAA; nt 23832 –

23839), with the latter matching the TRS-L sequence exactly. In this case, we found that Beaudette-derived chimeric reads could contain either a U (denoted "3/E [U3]") or a G (denoted "3/E [G3]"), with the G residue being slightly more common (1.6% versus 1.2%, respectively, on average); whereas M41-derived reads contained only the U residue (**Fig. 2A; Supp. Table S2**).

In agreement with a previous report (Stirrups et al., 2000), we found that the 3′-most of two adjacent canonical TRS-B sequences (both CUUAACAA; nt 25,460 – 25,467 and nt 25,471 – 25,478, labelled "5a/5b TRS 1" and "5a/5b TRS 2", respectively, in **Fig. 2A**) within the 30-nt region upstream of genes 5a/5b was preferentially utilised in IBV Beaudette; accounting for 18.8% of chimeric reads on average, compared with 1.5% for the 5′-most TRS-B. Interestingly, more chimeric reads were assigned to the non-canonical TRS-B associated with genes 4b/4c (Bentley et al., 2013) – which has a low homology to the TRS-L (**Supp. Table S2**) – than to the first of these 5a/5b-associated TRSs in IBV Beaudette; emphasising the importance of the genomic context in facilitating discontinuous transcription (**Fig. 2B** and **Fig. 2C**) (Sola et al., 2005). Only one of the two 5a/5b TRSs (TRS 2) is found in the IBV M41 genome (**Fig. 2A**).

**Novel TRS in IBV Beaudette**

Two additional non-canonical leader/body chimeras were identified, both specific to the Beaudette strain (**Supp. Table S2**). The more abundant of these (0.6% of chimeric reads) mapped to a position immediately downstream of the IBV Beaudette N gene termination codon, within the 3′ "untranslated" region (UTR). Chimeric reads derived from this site contained the sequence CUUAACAU; the last six nt of which could have been templated by the genomic (TRS-B) sequence (UAACAU, nt 27104 – 27109). There is an AUG-initiated downstream ORF (dORF) in Beaudette beginning two nt 3′ of this TRS, which comprises 11 codons (nt 27111 – nt 27143).

Inspection of our RiboSeq libraries shows that the dORF is ribosomally occupied (**Fig. 2D**). Such AUG-initiated dORFs are present immediately 3′ of the N genes in most IBV strains, and in TCoV, but this region appears to have been ancestrally deleted in the IBV M41 lineage; and M41 also lacks the TRS-B downstream of the N gene (UAAAAU, nt 27156 – 27161).

The second novel chimeric sequence identified in RNASeq libraries maps to a TRS-B (CUUACCAA) within the coding region of the S gene in Beaudette (nt 21242 – 21249). This is consistent with the previous detection of a sgmRNA of appropriate length via Northern blot analysis (Bentley et al., 2013). Whilst the core sequence of the TRS-B in this case is conserved in M41, there is a single nucleotide (A to C) polymorphism located four nt downstream in the 3′ flanking region, which may contribute to its lack of utilisation in this strain (**Supp. Table S2**).

**Virus translation: direct measurement of –1 PRF between ORF1a and ORF1b**

Ribosome profiling of eukaryotic systems typically has the characteristic that mappings of the 5′ end positions of RPFs to coding sequences reflect the triplet periodicity of genetic decoding. A clear phase transition is evident in the RiboSeq libraries at the junction of ORF1a and ORF1b; where frameshifting of a proportion of ribosomes from the former ORF into the latter occurs (**Fig. 3A and 3B**). The mean normalised ratios of ORF1b to ORF1a RiboSeq density were 0.32 and 0.37 in IBV Beaudette and IBV M41, respectively; while the corresponding RNASeq ratios were 0.97 and 0.94, respectively (**Fig. 3C**). Thus on average, 33% of ribosomes in Beaudette and 39% in M41 undergo –1 PRF prior to reaching the ORF1a termination codon (**Fig. 3D**). These values are very similar to those measured in *in vitro* PRF assays (Brierley et al., 1987, 1989) and alongside related profiling studies of MHV (Irigoyen et al., 2016), this indicates that coronaviruses exhibit highly efficient PRF both *in vitro* and in the context of the infected cell.

220

221 **Ribosomal occupancy of ORF4b and ORF4c**

222 Situated between the M and 5a genes in Beaudette and M41 is a >300-nt ostensibly “intergenic"
223 region (IGR) (**Fig. 1**). No protein-coding genes are annotated here but two putative AUG-initiated
224 ORFs are present in each virus, referred to as ORF4b and ORF4c, after their homologs in turkey
225 coronavirus [TCoV] (Gomaa et al., 2008; Cao et al., 2008) and in the genomes of most IBV isolates
226 (Reddy et al., 2015). The putative ORF4b genes of Beaudette and M41 are encoded by nt 25,183 –
227 25,335 (50 codons) and nt 25,190 – 25,474 (94 codons), respectively, of the gRNA; whereas the
228 ORF4c genes are encoded by nt 25,339 – 25,422 (27 codons) and nt 25,395 – 25,457 (20 codons),
229 respectively (**Supp. Fig. S9)**. Thus, in Beaudette, the two ORFs are separated by a 3-nt spacer
230 region and in the same reading frame (**Fig. 4A**); whereas in M41, ORF4c is located entirely within
231 the ORF4b gene and in the +1 phase (**Fig. 4B**). Inspection of the ribosomal profiling datasets
232 reveals substantial RPF coverage of both ORF4b and ORF4c, providing the first clear illustration
233 that ORFs 4b and 4c are ribosomally occupied **(Fig. 4)**. Visualisation of ORF4c translation in M41
234 was facilitated by good phasing in the datasets, allowing expression of both ORF4b and ORF4c to
235 be visualised (as both blue and orange RPF peaks in the overlap region). Previous work (Bentley et
236 al., 2013) has shown that a non-canonical TRS-B sequence – situated approximately 100 nt
237 upstream of the M gene termination codon – facilitates production of a sgmRNA that harbours
238 ORF4b at its 5′ end, and this TRS-B was also identified in our RNASeq data.

239

240 **Translation efficiencies of IBV genes**

241 To estimate the translational efficiency (TE) of virus genes, we summed RPFs whose 5′ end mapped
242 in-phase between the first nucleotide of the initiation codon and 30 nt 5′ of the termination codon;

thereby excluding RPFs derived from ribosomes paused during initiation or termination (Irigoyen et al., 2016). The TE of each ORF was measured as the quotient of the RPF density and the abundance of the corresponding mRNA; with separate calculations performed using the decumulated RNASeq densities and the TRS chimeric reads counts (**Fig. 5** and **Supp. Fig. S10**, respectively). In the case of ORF4b and ORF4c, transcript abundance could not be accurately deduced via the RNASeq decumulation procedure, because the significantly lower level of expression of the 4b/4c transcript relative to that of the 5′-adjacent M gene (**Fig. 1**) was associated with a proportionate increase in the level of noise. Similarly, as a result of the high abundance of gRNA relative to the sgmRNA encoding S, the decumulated RNASeq density for the latter is likely to be poorly estimated, and therefore the TE value for S calculated using the chimeric read count is likely to be more accurate. From this analysis, it was observed that the 4b gene is more efficiently translated than the 4c gene; a trend also observed for the accessory genes 3a/3b and 5a/5b (**Fig. 5**). This is consistent with the likely requirement for leaky scanning to access the downstream ORF on each sgmRNA (see Discussion). Surprisingly, despite the fact that the nucleocapsid (N) protein is an abundant viral protein, it was not found to be efficiently translated relative to the other structural proteins, regardless of the approach used to estimate transcript abundance (**Fig. 5; Supp. Fig. S10**). In the case of the ORF1a and ORF1b genes, a large proportion of the genomic RNA is expected to be destined for packaging rather than translation, as mentioned above, and this probably explains the low TE values calculated for these genes (**Fig. 5; Supp. Fig. S10**). Additionally, the short length of the dORF precluded an accurate assessment of its translation efficiency.

**Ribosomal pauses during IBV genome translation**

Inspection of the profiling datasets revealed a number of genomic locations where RPFs accumulated to a much higher level than at neighbouring sites, indicative of ribosomal pausing. As such pauses may have biological significance, we first sought to discount those that may have arisen artefactually. The known translation initiation sites in the virus genome generally showed high ribosome occupancy, but as the infected cells were treated with cycloheximide (CHX) prior to lysis to "freeze" ribosomes onto the mRNA, these pauses are likely to be over-represented, as ribosomes can accumulate at start codons during the CHX treatment period (Ingolia et al., 2011). Fluctuations in RPF density can also occur as a result of nuclease, ligation, and PCR biases during library construction. As the latter two biases can also occur during RNASeq library generation, we also discounted any pauses that had an obvious counterpart in RNASeq datasets. With these criteria, we identified five obvious sites of ribosomal pausing conserved in Beaudette and M41, one in the 5′ UTR and four within the coding region (indicated in **Fig. 1**, purple triangles; see **Table 1**). Pauses in 5′ UTRs can represent ribosomes initiating at upstream ORFs (uORFs), although in both Beaudette and M41, the P-site of the ribosome paused over bases 28–56 in the 5′ UTR of the genome is on a non-AUG codon (UUG) in a weak Kozak initiation consensus. As this pause is located upstream of the TRS_L, it reflects the sum of pausing on all sgmRNAs. To view the extent of the pause in context, we remapped reads to the most abundant sgmRNA, i.e. that of the N gene (**Fig. 6**). As can be seen, the "Leader pause" remains clearly evident (as is a smaller pause three codons downstream), albeit smaller in magnitude than those pauses seen at an N uORF (see below) and the authentic AUG codon of the N protein. Initiation at the UUG codon would result in translation of solely a dipeptide and thus the pause, if biologically relevant, may act as a regulator of downstream initiation events rather than through the encoded product. We note that an equivalent Leader pause is seen in MHV (UUG codon, 1-codon ORF; Irigoyen et al., 2016). It is possible that pausing at this codon is potentiated by queueing of initiating ribosomes on sgmRNAs. The origin of the pauses

within the coding region are enigmatic. The two adjacent pauses referred to collectively as Pause 2 in **Table 1** correspond to translation of a region of non-structural protein 4 (nsP4) downstream of the membrane spanning domains (Oostra et al., 2007; Doyle et al., 2018). It is feasible that ribosomes pause here whilst the nascent peptide is being folded into membranes. Pauses 3 and 4 are noticeably large and correspond to ribosomes pausing soon after initiation of the S and M proteins, respectively. In the case of the former, the pause appears to be unrelated to the signal sequence at the N-terminus of the S protein, since this would still be within the peptide exit tunnel of paused ribosomes. Pause 5 corresponds to a potential non-AUG uORF (AUU, in a reasonable context) within the N mRNA (**Fig. 6**).

It is noteworthy that in our analysis of ribosomal pause sites, we did not see pausing at the AUG of the previously described 11 amino acid uORF of the genomic mRNA (AUG at nt 131–133; Boursnell et al., 1987), and indeed there were few reads on the uORF itself, indicating that it is not heavily translated. Further, no pausing was observed at the PRF site at the ORF1a/ORF1b overlap.

**Differential expression of host genes in response to IBV infection**

We investigated the differential transcription and translation of host genes in response to IBV infection by comparing RNA and RPF densities per coding region for infected samples and mocks (see Materials and Methods). Details of the genes found to be differentially expressed (DEGs) (FDR < 0.05 with multiple testing correction using the Benjamini-Hochberg method) at the level of transcription (4,266 genes) or translation (3,627 genes) respectively, are provided in **Supp. Data Sets S1 and S2.** Overall, the patterns of change in host cell gene expression in response to infection were broadly similar for Beaudette and M41, with positive inter-strain correlations in the log2 fold changes (log2FC) in transcript abundance and translation efficiency ($R^2$ = 0.95 and $R^2$ = 0.85,

313 respectively, *P* values both < 2.2 × $10^{-16}$; **Fig. 7A**). Notably, the majority of differentially
314 transcribed genes were up-regulated rather than down-regulated (i.e. log2FC > 0) for both strains
315 (**Fig. 7A; left panel**), with 2.1-fold and 3.5-fold more up-regulated compared with down-regulated
316 transcripts (FDR <0.05; see Materials and Methods) detected in Beau-CK-infected cells and M41-
317 CK-infected cells, respectively (**Supp. Data Set S1**). This effect was not seen at the level of
318 translation, where there were fewer differentially expressed genes overall, and the logFC values of
319 those genes were more evenly distributed around 0, with slight skewing towards negative values
320 (i.e. reduced TE) (**Fig. 7A; right panel** and **Supp. Data Set S2**). The core host transcriptional
321 response to the two strains involved 579 commonly up-regulated and 132 commonly down-
322 regulated genes, while the core translational response consisted of 34 commonly up-regulated and
323 79 commonly down-regulated genes. Gene ontology (GO) term enrichment revealed that numerous
324 immune-related pathways were among the most significantly enriched terms in the core response
325 sets (**Fig. 7B** and **Fig. 7C**). There was also evidence of integration and coordination of responses at
326 the transcriptional and translational levels. For example, the GO term “positive regulation of NF-
327 kappaB transcription factor activity” (GO:0051092) was enriched among transcriptionally up-
328 regulated genes; whereas “negative regulation of NF-kappaB transcription factor activity”
329 (GO:0032088) was enriched among translationally down-regulated genes. In a direct inter-strain
330 comparison of statistically significant DEGs we identified 51 differentially transcribed genes, 45 of
331 which were more highly expressed in Beaudette-infected samples, and six of which were more
332 highly expressed in M41-infected samples (**Supp. Data Set S1**). The most significantly enriched
333 GO term in the former set was “regulation of signaling receptor activity” (GO:0010469); while pro-
334 proliferative and anti-apoptotic GO terms were also enriched (**Supp. Table S3**). The latter set
335 included three heat shock protein-encoding genes, and consequently the top enriched GO terms
336 were related to “protein refolding” (**Supp. Table S4**). Just one gene (ENSGALG00000015358

337 [MYH15], encoding myosin heavy chain 15) had a significantly higher translation efficiency in
338 M41-infected samples compared with Beaudette-infected samples.

339 In comparisons of host gene expression between Beaudette-, M41- and mock-infected cells, the
340 significantly differentially expressed genes (FDR <0.05) were ranked by log2FC (**Supp. Data Set**
341 **S3**) and the top 100 DEGs (or fewer) within each category were subjected to STRING analysis
342 (Szklarczyk et al., 2017) to identify potential protein-protein interaction pathways (**Fig. 8 and**
343 **Supp. Fig. S11)**. A selection of the key pathways proposed and examples of the associated genes
344 are shown in **Table 2**. Clear patterns of host response to virus infection were present that are
345 discussed below. Note in inter-strain comparisons of M41 versus Beaudette, only the
346 transcriptionally downregulated category had sufficient gene candidates for STRING analysis; the
347 other three categories had a total of only seven DEGs (thus no plots are shown in the **Supp**. **Info.**
348 for these).

349

350 **Discussion**

351 Here, we describe the first high-resolution study of gammacoronaviral gene expression during
352 infection of primary chick kidney cells. Analysis of RNASeq data sets through chimeric read
353 analysis or decumulation allowed us to quantify the relative levels of viral genomic and subgenomic
354 mRNAs and to define the sequence diversity of strain-specific TRS utilisation. The predominant
355 sgmRNA in both strains was that encoding the N protein, and between strains, the M transcript was
356 relatively more abundant in M41. In Beaudette, two novel TRS were identified, one in the viral 3′
357 UTR immediately downstream of the N gene termination codon, and one mapping to a TRS-B
358 within the S gene. In the former, a short ORF (dORF) – initiated two nt 3′ of the TRS – is present
359 and ribosomally occupied. The potential biological relevance of this ORF remains to be determined;

360 such dORFs are present in most IBV strains and in TCoV, but it is lacking in M41 (as is the TRS-
361 B). A recent report has described the same sgmRNA (initiating at the identical TRS) as a novel non-
362 coding RNA of IBV (An et al., 2019). The S gene TRS-B, proposed earlier (Bentley et al., 2013),
363 was also identified.

364 RiboSeq analysis, in conjunction with RNASeq, revealed that the N protein is not more efficiently
365 translated than other structural proteins, despite being a structural component of IBV virions.
366 Coronaviral N proteins are highly basic, reflecting the fact that they associate tightly with the
367 negatively charged gRNA (Laude et al., 1995), and a previous meta-analysis has indicated that the
368 decoding of positively charged amino acid residues is associated with a lowering in the speed of
369 translation (Charneski and Hurst 2013; Sabi & Tuller, 2015; Requiao et al., 2016). Thus, it is
370 possible that the relatively low TE of N is an unavoidable consequence of its amino acid
371 composition. N expression may also be regulated by a putative uORF whose initiation codon is
372 located some 50 nt upstream of the N AUG codon (**Fig. 6**).

373

374 The efficiency of PRF at the IBV ORF1a/ORF1b overlap in natural infection was found to be 33–
375 40%. This range is in close agreement with previous *in vitro* measurements of IBV frameshifting
376 efficiency carried out using reporter constructs (Brierley et al., 1989) and is consistent with the
377 notion that frameshifting in IBV is among the more efficient examples of canonical eukaryotic −1
378 PRF signals that have been studied to date (Atkins et al., 2016; Irigoyen et al., 2016). Whether the
379 modest difference in –1 PRF efficiency measured for Beau-CK and M41-CK has biological
380 significance is uncertain, and it may represent experimental variation. The frameshift signal of
381 M41-CK differs from Beau-CK in only three of 81 nucleotide positions, all of which are located in
382 loop 3 of the stimulatory pseudoknot and not expected to affect pseudoknot function or stability

(Brierley and Pennell, 2001). As also described for MHV-infected cells (Irigoyen et al., 2016), there was no evidence that the frameshift-stimulatory pseudoknot induced ribosomal pausing on the slippery sequence. Thus pausing may not be a component of the frameshifting mechanism, or the pause may be too short-lived to be visualised by the profiling technique.

A meta-analysis of host genes revealed highly specific phasing of the RiboSeq data sets, enabling the accurate determination of the reading frame of translation for individual RPFs. Good phasing in the datasets and substantial read depth also allowed us to examine translation of viral accessory ORFs. It was evident that both 4b and 4c are efficiently translated, at levels comparable to those of the 5a/5b accessory protein-encoding genes. The mechanism by which ribosomes might access ORF4c, however, is not clear. Given the absence of AUG codons within the regions between the 5′ ends of ORF4b and ORF4c in both Beaudette and M41 (**Supp. Fig. S9**), and the weak initiation context of the ORF4b start codon, it is possible that a proportion of ribosomes might bypass the ORF4b initiation codon and instead translate ORF4c via “leaky scanning” (Firth and Brierley, 2012), although it should be noted that intervening AUG codons do exist in some other IBV strains (**Supp. Fig. S9**).

The relevance to virus gene expression of the sites of significant ribosomal pausing identified in the genome remains to be investigated experimentally. Two of these pause sites appear to correspond to uORFs initiated at non-AUG initiation codons, one in the 5′ UTR and one upstream of the N gene. In each case, ribosomes initiating on the main ORF AUG (ORF1a and N respectively) could potentiate initiation on the uORFs through stacking of scanning ribosomes, and this could be artefactually increased by the cycloheximide pretreatment used during sample preparation. Two of

406 the other pause sites correspond to ribosomes paused post-initiation early in the coding regions of
407 the S and M genes. A biological explanation for this is lacking at present. We are aware that the
408 treatment of yeast cells with cycloheximide can lead to an early block in elongation in stressed cells
409 (Gerashchenko and Gladyshev, 2014; Duncan and Mata, 2017), but meta-analysis of host genes in
410 our infected cells does not reveal an obvious elongation block. Further, the S and M genes show
411 deep ribosome coverage along their lengths, inconsistent with a block in elongation. The remaining
412 pause site (in fact a doublet) appears during translation of the nsP4 region of the polyprotein close
413 to the C-terminus of nsP4. Coronaviral nsP4 proteins are important for the membrane
414 rearrangements required for viral RNA synthesis and contain multiple membrane spanning domains
415 (Doyle et al., 2018). A possible explanation for the ribosomal pauses seen here is that translation is
416 paused to permit the correct folding of nsP4 into membranes.

417

418 In general, the pauses we discern during translation of the IBV genome are discrete, substantial in
419 terms of read counts, and reproducible. As mentioned above, their origin is uncertain, but it seems
420 unrelated to the identity of the P-site tRNA. Recent studies have shown that P-site prolyl-tRNA is a
421 strong determinant of ribosomal pausing, partly due to the slow rate of peptide bond formation with
422 this amino acid (Sabi and Tuller, 2015; 2017). However, none of the stall sites identified here have
423 proline tRNA in the P-site. One possible explanation we cannot rule out is that some feature of the
424 nascent peptide engenders pausing through interactions with the ribosome exit tunnel or
425 chaperones; clusters of positively-charged amino acid residues have been documented to induce
426 ribosome pausing (Ingolia, 2014; Sabi and Tuller, 2017), although such clusters are not evident
427 upstream of the pause sites seen here. The recent developments of methodologies and algorithms to
428 identify and characterise ribosomal pause sites may clarify the situation in future (Chadani et al.,
429 2016; Kumari et al., 2018).

Our data indicate that the host response to IBV is mediated primarily at the level of transcription, with the up-regulation of hundreds of genes, many of which have immune-related functions. Changes in translational efficiency were more modest, with more genes showing decreased rather than increased translation in response to IBV infection. Many of the transcriptionally upregulated genes identified reflect the host response to virus infection, as seen previously with IBV infection of chickens (Cong et al., 2013; Chhabra et al., 2018) and with other RNA viruses (Zhang et al., 2018). Some of the protein pathways identified have not been associated with coronavirus infection previously and warrant experimental follow up, for example, the potential downregulation of transcription of genes linked to FAM20C, a kinase that generates the majority of the extracellular phosphoproteome (Tagliabracchi et al., 2015). Also of interest is the translational upregulation of ribosomal protein synthesis in infected cells for both Beau-CK and M41-CK. A direct comparison of DEGs in M41-CK and Beau-CK-infected primary chick kidney cells did not identify any obvious pathways that would reflect their differential pathogenesis. Overall, these data contribute towards a substantially improved understanding of the early innate immune response to IBV infection, including distinct features of the transcriptional and translational responses.

## MATERIALS AND METHODS

**Virus and cells:** The apathogenic molecular clone of IBV, Beau-R, has been described previously (Casais et al., 2001) and was used to generate virus Beau-CK. The pathogenic isolate M41-CK has been described previously (Kottier et al., 1995). Primary chick kidney (CK) cells were produced from 2–3 week-old specific pathogen free (SPF) Rhode Island Red chickens (Hennion and Hill, 2015). CK cells ($0.8 \times 10^6$ cells/ml) were plated in 10-cm dishes and upon reaching 100%

confluence (two days post-seeding) were washed once with PBS and infected with $9.6 \times 10^6$ PFU Beau-CK or M41-CK. After 1 hour incubation at 37 °C, 5% $CO_2$, the inoculum was removed and replaced with 10 ml fresh 1x BES (1X minimal essential Eagle's medium [MEM], 0.3% tryptose phosphate broth, 0.2% bovine serum albumin, 20 mM N,N-Bis(2-hydroxyethyl)-2-aminoethanesulfonic acid (BES), 0.21% sodium bicarbonate, 2 mM L-glutamine, 250 U/ml nystatin, 100 U/ml penicillin, and 100 U/ml streptomycin). Cells were harvested at 24 hours post-infection when clear regions of cytopathic effect (CPE) were visible.

**Drug treatment, cell harvesting and lysis:** Cycloheximide (CHX; Sigma-Aldrich) was added directly to the growth medium (to 100 µg/ml) and the cells incubated for 2 min at 37 °C before rinsing with 5 ml of ice-cold PBS containing CHX (100 µg/ml). Subsequently, dishes were incubated on ice and 400 µl of lysis buffer [20 mM Tris-HCl pH 7.5, 150 mM NaCl, 5 mM $MgCl_2$, 1 mM DTT, 1% Triton X-100, 100 µg/ml cycloheximide and 25 U/ml TURBO™ DNase (Life Technologies)] dripped onto the cells. The cells were scraped extensively to ensure lysis, collected and triturated with a 26-G needle ten times. Lysates were clarified by centrifugation for 20 min at 13,000 g at 4 °C, the supernatants recovered and stored at −80 °C.

**Ribosomal profiling and RNASeq:** Cell lysates were subjected to RiboSeq and RNASeq. The methodologies employed were based on the original protocols of Ingolia and colleagues (Ingolia et al., 2009; 2012), except ribosomal RNA contamination was removed using a commercial RiboZero Gold magnetic kit (Illumina) and library amplicons were constructed using a small RNA cloning strategy (Guo et al., 2010) adapted to Illumina smallRNA v2 to allow multiplexing. The methods used were as described by Chung et al. (2015), except the 5′ and 3′ adapters included seven consecutive randomised bases at the 3′ and 5′ ends (respectively). This facilitated removal of reads

duplicated during polymerase chain reaction (PCR) amplification of cDNA libraries (Aird et al; 2011) and reduced ligation bias. Amplicon libraries were deep sequenced using an Illumina NextSeq platform (Department of Pathology, University of Cambridge).

**Computational analysis of RiboSeq and RNASeq data**

Adaptor sequences were trimmed using FASTX-Toolkit (hannonlab.cshl.edu/fastx_toolkit), and reads shorter than 25 nt following adaptor trimming were discarded. Mapping was performed using Bowtie version 1 (Langmead et al., 2009) with parameters -v 2 --best (i.e. maximum 2 mismatches, report best match). Adaptor-trimmed, de-duplicated reads were mapped sequentially to host (*Gallus gallus*) ribosomal RNA (rRNA); IBV Beaudette (GenBank accession: NC_001451.1) or IBV M41 (GenBank accession: DQ834384.1) gRNA; Ensembl host non-coding RNA (ncRNA); NCBI RefSeq host mRNA; and to the host genome . The order of mapping was tested to check that virus-derived reads were not lost accidentally due to mis-mapping to host RNA, or *vice versa*. When performing analyses of viral and host gene expression, only 28- and 29-nt RiboSeq reads (corresponding to RPFs mapping primarily in phase 0) and only ≥ 40 nt RNASeq reads were used. A 12-nt offset was applied to the 5′ mapping positions of RPFs, to approximate the P-site position of the ribosome (see **Supp. Fig. S4** and Irigoyen et al., 2016). To normalize for different library sizes, reads per million mapped reads (RPM) values were calculated using the sum of total virus RNA plus total host RefSeq mRNA (positive sense reads only) as the denominator.

Host mRNA RiboSeq and RNASeq phasing distributions were derived from reads mapping internally to the coding regions of ORFs; specifically, the 5′ end of the read had to map between the first nucleotide of the initiation codon and 30 nt 5′ of the last nucleotide of the termination codon, thus, in general, excluding RPFs of initiating or terminating ribosomes. Histograms of 5′ end

positions of host mRNA reads relative to initiation and termination codons (Supp. Figs. 4 – 7) were derived from reads mapping to RefSeq mRNAs with annotated CDSs at least 450 nt in length and annotated 5′ and 3′ UTRs at least 60 nt in length. When calculating the translation efficiencies of viral genes, only in-phase (i.e. phase 0 with respect to the ORF in question) RiboSeq reads were counted.

For host differential expression analyses, non-ribosomal, non-viral reads in each library were mapped to the *Gallus gallus* 5.0 assembly (December 2015) using STAR (Dobin et al., 2013), with gene annotations from Ensembl release 94 (Cunningham et al., 2019). A maximum of two mismatches were allowed when mapping. Read counts per gene (protein-coding genes only) were obtained using HTSeq (Anders et al., 2015), with a requirement that reads map entirely within the forward strand coding sequence (htseq-count parameters: -m intersection-strict -s yes -t CDS). For each comparison of experimental groups, only genes with an average of at least 50 mapped reads were included in differential expression analyses. GO term enrichment analysis was carried out using the topGO package in R (Alexa and Rahnenfuhrer, 2018) and Fisher's exact test was used to assess the enrichment of individual GO terms in specific gene lists. Protein-protein interaction networks were constructed using the Search Tool for Retrieval of Interacting Genes (STRING) database (Szklarczyk et al., 2017).

**Acknowledgements**

This work was supported by UK Medical Research Council [MR/M011747/1] and Wellcome Trust [202797/Z/16/Z] grants to I.B. and Wellcome Trust grant [106207] and European Research Council (ERC) European Union's Horizon 2020 research and innovation programme grant [646891] to A.E.F.

525

526 **References**

527 Aird, D., Ross, M.G., Chen, W.S., Danielsson, M., Fennell, T., Russ, C., Jaffe, D.B., Nusbaum, C.
528 and Gnirke, A. (2011). Analyzing and minimizing PCR amplification bias in Illumina sequencing
529 libraries. Genome Biol. 12: R18.

530

531 Alexa A, Rahnenfuhrer J (2018). *topGO: Enrichment Analysis for Gene Ontology*. R package
532 version 2.34.0.

533

534 Alonso-Caplen, F.V., Matsuoka, Y., Wilcox, G.E. and Compans, R.W. (1984). Replication and
535 morphogenesis of avian coronavirus in Vero cells and their inhibition by monensin. Virus Res.
536 1:153-167.

537

538 An, H., Cai, Z., Yang ,Y., Wang, Z., Liu, D.X. and Fang, S. (2019). Identification and formation
539 mechanism of a novel noncoding RNA produced by avian infectious bronchitis virus. Virology
540 528:176-180.

541

542 Anders, S., Pyl, P.T. and Huber, W. (2015). HTSeq - a Python framework to work with high-
543 throughput sequencing data. Bioinformatics 31:166-169.

544

545 Atkins, J.F., Loughran, G., Bhatt, P.R., Firth, A.E. and Baranov, P.V. (2016). Ribosomal
546 frameshifting and transcriptional slippage: From genetic steganography and cryptography to
547 adventitious use. Nucleic Acids Res. 44:7007-7078.

548

549 Beaudette, F. R. and Hudson C. R. (1937). Cultivation of the virus of infectious bronchitis. J. Am.
550 Vet. Med. Assoc. 90: 51–60.
551
552 Bentley, K., Keep, S.M., Armesto, M. and Britton, P. (2013). Identification of a noncanonically
553 transcribed subgenomic mRNA of infectious bronchitis virus and other gammacoronaviruses.
554 J .Virol. 87: 2128-2136.
555
556 Bickerton, E., Maier, HJ., Stevenson-Leggett, P., Armesto, M. and Britton, P. (2018). The S2
557 Subunit of Infectious Bronchitis Virus Beaudette Is a Determinant of Cellular Tropism. J. Virol. 92.
558 pii: e01044-18.
559
560 Boursnell, M.E., Brown, T.D., Foulds, I.J., Green, P.F., Tomley, F.M., Binns, M.M. (1987).
561 Completion of the sequence of the genome of the coronavirus avian infectious bronchitis virus. J.
562 Gen. Virol. 68:57-77.
563
564 Brierley, I., Boursnell, M.E., Binns, M.M., Bilimoria, B., Blok, V.C., Brown, T.D. and Inglis, S.C.
565 (1987). An efficient ribosomal frame-shifting signal in the polymerase-encoding region of the
566 coronavirus IBV. EMBO J. 6: 3779-3785.
567
568 Brierley, I, Digard, P. and Inglis, S.C. (1989). Characterization of an efficient coronavirus ribosomal
569 frameshifting signal: requirement for an RNA pseudoknot. Cell 57: 537-547.
570

571 Brierley I. and Pennell, S. (2001). Structure and function of the stimulatory RNAs involved in
572 programmed eukaryotic-1 ribosomal frameshifting. Cold Spring Harb. Symp. Quant. Biol. 66: 233-
573 248.
574
575 Brockway, S.M, Clay, C.T., Lu, X.T. and Denison, M.R. (2003). Characterization of the expression,
576 intracellular localization, and replication complex association of the putative mouse hepatitis virus
577 RNA-dependent RNA polymerase. J. Virol. 77: 10515-10527.
578
579 Brown, T.D., Boursnell, M.E., Binns, M.M. and Tomley, F.M. (1986). Cloning and sequencing of 5'
580 terminal sequences from avian infectious bronchitis virus genomic RNA. J. Gen. Virol. 67:221-228.
581
582 Cao, J., Wu, C.C. and Lin, T.L. (2008). Complete nucleotide sequence of polyprotein gene 1 and
583 genome organization of turkey coronavirus. Virus Res. 136: 43-49.
584
585 Casais, R., Dove, B., Cavanagh D. and Britton, P. (2003). Recombinant avian infectious bronchitis
586 virus expressing a heterologous spike gene demonstrates that the spike protein is a determinant of
587 cell tropism. J. Virol. 77: 9084-9089.
588 Casais, R., Thiel, V., Siddell, S.G., Cavanagh, D. and Britton, P. (2001). Reverse genetics system for
589 the avian coronavirus infectious bronchitis virus. J. Virol. 75, 12359–12369.
590
591 Cavanagh, D. (2005). Coronaviruses in poultry and other birds. Avian Pathol. 34: 439-448.
592
593 Cavanagh, D. (2007). Coronavirus avian infectious bronchitis virus. Vet. Res. 38: 281-297.
594

595 Chadani, Y., Niwa, T., Chiba, S., Taguchi, H. and Ito, K. (2016). Integrated *in vivo* and *in vitro*
596 nascent chain profiling reveals widespread translational pausing. Proc. Natl. Acad. Sci. U.S.A.
597 113:E829-38.
598
599 Chhabra, R., Ball, C., Chantrey, J. and Ganapathy, K. (2018). Differential innate immune responses
600 induced by classical and variant infectious bronchitis viruses in specific pathogen free chicks. Dev.
601 Comp. Immunol. 87:16-23.
602
603 Charneski, C.A. and Hurst, L.D. (2013). Positively charged residues are the major determinants of
604 ribosomal velocity. PLoS Biol. 11:e1001508.
605
606 Chung, B.Y., Hardcastle, T.J.,, Jones J..D, Irigoyen,. N, Firth ,A.E., Baulcombe, D.C. and Brierley,
607 I. (2015). The use of duplex-specific nuclease in ribosome profiling and a user-friendly software
608 package for Ribo-seq data analysis. RNA 21:1731-1745.
609
610 Cong, F., Liu, X.,, Han Z., Shao, Y., Kong, X. and Liu, S. (2013). Transcriptome analysis of chicken
611 kidney tissues following coronavirus avian infectious bronchitis virus infection. BMC Genomics
612 14:743.
613
614 Cunningham, C.H., Spring, M.P. and Nazerian, K. (1972). Replication of avian infectious bronchitis
615 virus in African green monkey kidney cell line VERO. J. Gen. Virol. 16: 423-427.
616
617 Cunningham, F., Achuthan, P., Akanni, W., Allen, J., Amode, M.R., Armean, I.M., Bennett, R.,
618 Bhai, J., Billis, K., Boddu, S. et al. (2019). Ensembl 2019. Nucleic Acids Res. 47:D745-D751.

Dobin, A., Davis, C.A., Schlesinger, F., Drenkow, J., Zaleski, C., Jha, S., Batut, P, Chaisson, M. and Gingeras, T.R. (2013). STAR: ultrafast universal RNA-seq aligner. Bioinformatics 29:15-21.

Doyle, N., Neuman, B.W., Simpson, J., Hawes, P.C., Mantell, J., Verkade, P., Alrashedi, H. and Maier, H.J. (2018). Infectious Bronchitis Virus Nonstructural Protein 4 Alone Induces Membrane Pairing. Viruses 10 pii: E477.

Duncan, C.D.S. and Mata, J. (2017). Effects of cycloheximide on the interpretation of ribosome profiling experiments in Schizosaccharomyces pombe. Sci. Rep. 7:10331.

Firth, A.E. and Brierley, I. (2012). Non-canonical translation in RNA viruses. J. Gen. Virol. 93:1385-1409.

Fuchs, R.T., Sun, Z., Zhuang, F. and Robb, G.B (2015). Bias in ligation-based small RNA sequencing library construction is determined by adaptor and RNA structure. PLoS One. 10: e0126049.

Gerashchenko, M.V. and Gladyshev, V.N. (2014). Translation inhibitors cause abnormalities in ribosome profiling experiments. Nucleic Acids Res. 42:e134.

Gomaa, M.H., Barta, J.R., Ojkic, D. and Yoo, D. (2008). Complete genomic sequence of turkey coronavirus. Virus Res. 135: 237-246.

643 Gorbalenya, A.E , Enjuanes, L., Ziebuhr, J. and Snijder E.J. (2006). Nidovirales: evolving the
644 largest RNA virus genome. Virus Res. 117: 17-37.
645
646 Hennion, R. and Hill, G. (2015). In *Coronaviruses* Vol. 1282 *Methods in Molecular Biology* (eds
647 Helena Jane Maier, Erica Bickerton, & Paul Britton) Ch. 6, 57–62. (Springer New York).
648
649 Hodgson, T., Casais, R., Dove, B., Britton, P. and Cavanagh, D. (2014). Recombinant infectious
650 bronchitis coronavirus Beaudette with the spike protein gene of the pathogenic M41 strain remains
651 attenuated but induces protective immunity. J. Virol. 78: 13804-13811.
652
653 Ingolia, N.T., Ghaemmaghami, S., Newman, J.R. and Weissman, J.S. (2009). Genome-wide
654 analysis in vivo of translation with nucleotide resolution using ribosome profiling. Science. 324:
655 218-223.
656
657 Ingolia, N.T., Lareau, L.F. and Weissman, J.S. (2011). Ribosome profiling of mouse embryonic
658 stem cells reveals the complexity and dynamics of mammalian proteomes. Cell. 147: 789-802.
659
660 Ingolia, N.T., Brar, G.A., Rouskin, S., McGeachy, A.M. and Weissman, J.S. (2012). The ribosome
661 profiling strategy for monitoring translation in vivo by deep sequencing of ribosome-protected
662 mRNA fragments. Nat. Protoc. 7:1534-1550.
663
664 Ingolia, N.T. (2014). Ribosome profiling: new views of translation, from single codons to genome
665 scale. Nat. Rev. Genet. 15:205-213.
666

667 Irigoyen, N., Firth, A.E., Jones, J.D., Chung, B.Y., Siddell, S.G and Brierley, I. (2016). High-
668 resolution analysis of coronavirus gene expression by RNA sequencing and ribosome profiling.
669 PLoS Pathog. 12:e1005473.
670
671 Irigoyen, N., Dinan, A.M., Brierley, I. and Firth, A.E. (2018). Ribosome profiling of the retrovirus
672 murine leukemia virus. Retrovirology 15: 10.
673
674 Jukes, T.H. (1996). On the prevalence of certain codons ("RNY") in genes for proteins. J. Mol.
675 Evol. 42:3 77-381.
676
677 Kottier, S.A., Cavanagh, D. and Britton, P. (1995). Experimental evidence of recombination in
678 coronavirus infectious bronchitis virus. Virology. 213:569-580.
679
680 Kumari, R., Michel, A.M. and Baranov, P.V. (2018). PausePred and Rfeet: webtools for inferring
681 ribosome pauses and visualizing footprint density from ribosome profiling data. RNA 24:1297-
682 1304.
683
684 Kuo, L. and Masters, P.S. (2013). Functional analysis of the murine coronavirus genomic RNA
685 packaging signal. J. Virol. 87:5182-5192.
686
687 Langmead, B., Trapnell, C., Pop, M. and Salzberg, S.L. (2009). Ultrafast and memory-efficient
688 alignment of short DNA sequences to the human genome. Genome Biol. 10: R25.
689

690 Laude, Hubert, and Paul S. Masters. "The coronavirus nucleocapsid protein." *The Coronaviridae*.
691 Springer US, 1995. 141-163.
692
693 Liu, D.X., Xu, H.Y. and Brown, T.D. (1997). Proteolytic processing of the coronavirus infectious
694 bronchitis virus 1a polyprotein: identification of a 10-kilodalton polypeptide and determination of
695 its cleavage sites. J Virol. 71:1814-1820.
696
697 Oostra, M., te Lintelo, E.G., Deijs, M., Verheije, M.H., Rottier, P.J. and de Haan, C.A. (2007).
698 Localization and membrane topology of coronavirus nonstructural protein 4: involvement of the
699 early secretory pathway in replication. J. Virol. 81:12323-12336.
700
701 Otsuki, K., Noro, K., Yamamoto, H. and Tsubokura, M. (1979). Studies on avian infectious
702 bronchitis virus (IBV). II. Propagation of IBV in several cultured cells. Arch. Virol. 60: 115-122.
703
704 Pasternak, A.O., van den Born, E., Spaan, W.J. and Snijder, E.J. (2001). Sequence requirements for
705 RNA strand transfer during nidovirus discontinuous subgenomic RNA synthesis. EMBO J. 20:
706 7220-7228.
707
708 Reddy, V.R., Theuns, S., Roukaerts, I.D., Zeller, M., Matthijnssens, J. and Nauwynck, H.J. (2015).
709 Genetic Characterization of the Belgian Nephropathogenic Infectious Bronchitis Virus (NIBV)
710 Reference Strain B1648. Viruses 7: 4488-4506.
711

712 Requião, R.D., de Souza, H.J., Rossetto, S., Domitrovic, T. and Palhano, F.L. (2016). Increased
713 ribosome density associated to positively charged residues is evident in ribosome profiling
714 experiments performed in the absence of translation inhibitors. RNA Biol. 13:561-568.
715
716 Sabi, R. and Tuller T. (2015). A comparative genomics study on the effect of individual amino acids
717 on ribosome stalling. BMC Genomics 16 Suppl. 10:S5.
718
719 Sabi, R. and Tuller, T. (2017). Computational analysis of nascent peptides that induce ribosome
720 stalling and their proteomic distribution in *Saccharomyces cerevisiae*. RNA 23:983-994.
721
722 Sawicki, S.G. and Sawicki, D.L. (1995). Coronaviruses use discontinuous extension for synthesis of
723 subgenome-length negative strands. Adv. Exp. Med. Biol. 380: 499-506.
724
725 Sawicki, S.G. and Sawicki, D.L. (1998). A new model for coronavirus transcription. Adv. Exp.
726 Med. Biol. 440: 215-219.
727
728 Sawicki, S.G., Sawicki, D.L. and Siddell, S.G. (2007). A contemporary view of coronavirus
729 transcription. J. Virol. 81: 20-29.
730
731 Stewart, H., Brown, K., Dinan, A.M., Irigoyen, N., Snijder, E.J. and Firth, A.E. (2018).
732 Transcriptional and translational landscape of equine torovirus. J. Virol. 92 pii: e00589-18.
733

734 Sola, I., Moreno, J.L., Zúñiga, S., Alonso, S. and Enjuanes, L. (2005). Role of nucleotides
735 immediately flanking the transcription-regulating sequence core in coronavirus subgenomic mRNA
736 synthesis. J. Virol. 79: 2506-2516.
737
738 Stern-Ginossar, N. (2015). Decoding viral infection by ribosome profiling. J. Virol. 89: 6164-6166.
739
740 Stirrups, K., Shaw, K., Evans, S., Dalton, K., Casais, R., Cavanagh, D. and Britton, P. (2000).
741 Expression of reporter genes from the defective RNA CD-61 of the coronavirus infectious
742 bronchitis virus. J. Gen. Virol. 81:1687-1698.
743
744 Szklarczyk, D., Morris, J.H., Cook, H., Kuhn, M., Wyder, S., Simonovic, M., Santos, A., Doncheva,
745 N.T., Roth, A., Bork, P., Jensen, L.J. and von Mering, C. (2017). The STRING database in 2017:
746 quality-controlled protein-protein association networks, made broadly accessible. Nucleic Acids
747 Res. 45(D1):D362-D368.
748
749 Tagliabracci, V.S., Wiley, S.E., Guo, X., Kinch, L.N., Durrant, E., Wen, J., Xiao, J., Cui, J., Nguyen,
750 K.B., Engel, J.L., Coon, J.J., Grishin, N., Pinna, L.A., Pagliarini, D.J. and Dixon, J.E. (2015). A
751 Single Kinase Generates the Majority of the Secreted Phosphoproteome. Cell 161:1619-1632.
752
753 Van Roekel, H., Clarke, M.K., Bullis, K.L., Olesiuk, O.M. and Sperling, F.G. (1951). Infectious
754 bronchitis. Am. J. Vet. Res. 12:140-146.
755
756 Wolin, S.L. and Walter, P. (1988). Ribosome pausing and stacking during translation of a eukaryotic
757 mRNA. EMBO J. 7: 3559-3569.

Zhang, J., Kaiser, M.G., Deist,. MS., Gallardo, R.A., Bunn, D.A., Kelly, T.R., Dekkers, J.C.M., Zhou, H.and Lamont, S.J. (2018). Transcriptome analysis in spleen reveals differential regulation of response to Newcastle disease virus in two chicken lines. Sci. Rep. 8:1278.

Zúñiga, S., Sola, I., Alonso, S. and Enjuanes, L. (2004). Sequence motifs involved in the regulation of discontinuous coronavirus subgenomic RNA synthesis. J. Virol. 78: 980-994.

## FIGURE LEGENDS

**Figure 1. Structure and read coverage of the (A) IBV Beaudette and (B) IBV M41 genomes.** Coverage in the RiboSeq (red) and RNASeq (green) libraries is plotted on a logarithmic scale. The 5′ two-thirds of the IBV gRNA contains two large ORFs encoding pp1a and pp1b, respectively. Translation of the latter requires −1 programmed ribosomal frameshifting (PRF) at the indicated site. A nested set of 3′-coterminal sgmRNAs is produced during infection. Diamond symbols show the locations of canonical TRSs at which discontinuous transcription occurs (TRS-L in orange and TRS-B in green). Downward arrows indicate the positions of non-canonical TRSs discussed in this work. Purple triangles indicate sites of ribosomal pausing (see text).

**Figure 2. (A)** Proportion of chimeric reads assigned to each of the indicated TRS junctions. Novel TRS identified in this study are indicated with asterisks. Note that the 5a/5b TRS 1 and the dORF TRS are present in IBV Beaudette only. **(B)** Sequence logo depicting nucleotides surrounding the identified TRS-B sites in IBV Beaudette. **(C)** Equivalent sequence logo for IBV M41. **(D)** RiboSeq

781 and RNASeq coverage of the IBV Beaudette dORF. The location of the novel TRS-B sequence,
782 which begins 2 nt 3′ of the N gene termination codon, is indicated with an arrow. Coverage is
783 expressed as reads per million mapped reads (RPM). Reads in phase 0, +1, and +2 relative to the N
784 gene ORF are shown in blue, purple, and orange, respectively; and ORFs are coloured according to
785 the frame in which they are encoded.

786

787 **Figure 3.** RiboSeq and RNASeq coverage proximal to the junction between ORF1a and ORF1b for
788 IBV Beaudette **(A)** and IBV M41 **(B)**.-The last 2,500 nt of ORF1a and first 2,500 nt of ORF1b are
789 shown. Coverage is normalised to reads per million mapped reads (RPM), and smoothed with a
790 121-codon sliding window. Reads in phase 0, +1, and +2 relative to ORF1a are shown in blue,
791 purple, and orange, respectively; and ORFs are coloured according to the frame in which they are
792 encoded. **(C)** Ratios of ORF1b to ORF1a read density expressed as reads per kilobase per million
793 mapped reads (RPKM). RPKM values exclude the 150-nt regions downstream of the ORF1a
794 initiation codon, upstream of the ORF1b termination codon, and either side of the frameshift site.
795 **(D)** Frameshifting efficiencies calculated using the values plotted in **(C)**.

796

797 **Figure 4.** RiboSeq and RNASeq coverage of ORF4b and ORF4c in **(A)** IBV Beaudette and **(B)** IBV
798 M41. Coverage is expressed as reads per million mapped reads (RPM). Reads in phase 0, +1, and
799 +2 relative to ORF4b are shown in blue, purple, and orange, respectively; and ORFs are coloured
800 according to the frame in which they are encoded.

801

802 **Figure 5.** Translation efficiencies of viral genes, as calculated using the relative abundances (reads
803 per million, RPM) of chimeric TRS-spanning RNASeq reads. Values shown are relative to the mean
804 efficiency per TRS.

805

806 **Figure 6.** RiboSeq and RNASeq coverage of sgmRNA N in IBV Beaudette. Coverage is expressed
807 as reads per million mapped reads (RPM). Reads in phase 0, +1, and +2 relative to N are shown in
808 purple, orange and blue, respectively; and ORFs are coloured according to the frame in which they
809 are encoded.

810

811 **Figure 7. (A)** Log2 fold changes (log2FC) in host transcript abundance and translation efficiency in
812 infected cells relative to mocks. In both cases, a high degree of correlation was observed between
813 logFC values in Beaudette-infected samples (*x*-axes) and M41-infected samples (*y*-axes), with
814 transcript abundances skewed towards positive log2FC values. **(B)** The ten most significantly
815 enriched GO terms among commonly up-regulated (left panel) and commonly down-regulated
816 (right panel) genes at the level of transcription. **(C)** The ten most significantly enriched GO terms
817 among commonly up-regulated (left panel) and commonly down-regulated (right panel) genes at the
818 level of translation efficiency.

819

820 **Figure 8.** STRING analysis of the relationship between differentially expressed transcripts in
821 comparisons of IBV M41- and mock-infected cells. **(A)** Downregulated genes **(B)** Upregulated
822 genes. The network nodes represent the proteins encoded by the differentially expressed genes.
823 Seven different coloured lines link a number of nodes and represent seven types of evidence used in
824 predicting associations. A red line indicates the presence of fusion evidence; a green line represents

825 neighborhood evidence; a blue line represents co-ocurrence evidence; a purple line represents
826 experimental evidence; a yellow line represents text-mining evidence; a light blue line represents
827 database evidence; and a black line represents co-expression evidence.
828
829
830 **DATA AVAILABILITY**
831 Sequencing data have been deposited in ArrayExpress (http://www.ebi.ac.uk/arrayexpress) under
832 the accession number E-MTAB-7849.

833 **Table 1.** Ribosomal pause sites within the IBV genome.

834

| Pause | Genomic location and RPF sequence | Nascent peptide |
|---|---|---|
| Pause 1 (5′NCR) | 5′ end of genome (bases 28–56) near TRS_L<br>5′ AUUACACUAGCCUUGCGCUAGAUUUUUA 3′ | *YISITLALR* |
| Pause 2 (nsP4) | Two adjacent peaks within nsP4 coding region (~8660 and 8760)<br>5′ UUUGUUAAGCUUACUAAUGAGAUAGGU 3′<br>5′ UUGCAAGCUUGUCGUGCAUGGUUAGCU 3′ | YDGNEFVGNYDLAAKSTFVIRGSEFVKLTN<br>KFEAYLSAYARLKYYSGTGSEQDYLQACRA |
| Pause 3 (S) | Large pause downstream of initiation codon of S protein (~20,410)<br>5′ CUAGUGACUCUUUUGUGUGCACUAUGU 3′ (Beau) | †MLVTPLLLVTLLC (Beau) |
| Pause 4 (M) | Very large pause immediately downstream of initiation codon of the M protein (~24,500)<br>5′ (AUG)CCCAACGAGACAAAUUGUACUCUUGACU 3′. | †MPNETNC |
| Pause 5 (N) | Broad pause peak centered on YLSSIPREN near end of 5b ORF (~25,830), just upstream of N start codon ribosome stack<br>5′ UACCUCUCUAGUAUUCCAAGGGAAAACU 3′ | QSRTSRALSRVYLSSIP(RENL*) |

835

836 Underlined characters signify codon/amino acid of the ribosomal P-site tRNA.

837 * in-frame stop codon.

838 † initiator methionine

839

840

841

842

843

844

845

846

847

848

849 **Table 2**. STRING analysis of differential gene expression.

850

| Comparison | Parameter | Main pathway(s) | Examples in pathway(s) (FDR; log2fc) |
|---|---|---|---|
| ***Transcription*** | | | |
| Beaudette vs Mock | Downregulated | FAM20C substrates | SPP1 (secreted phosphoprotein 1) ($7.31 \times 10^{-15}$; –2.72).<br>TF (transferrin) ($1.83 \times 10^{-13}$; –3.17). |
| M41 vs Mock | Downregulated | FAM20C substrates | SPP1 (secreted phosphoprotein 1) ($6.13 \times 10^{-10}$; –3.177).<br>CHGB (chromogranin B) ($7.42 \times 10^{-8}$; –2.09). |
| Beaudette vs Mock | Upregulated | Antiviral state, receptor signalling, cytokine interactions | RSAD2 (viperin) ($3.92 \times 10^{-155}$; 9.49).<br>IFIT5 (interferon induced protein with tetratricopeptide repeats 5) ($4.48 \times 10^{-142}$; 8.66). |
| M41 vs Mock | Upregulated | Antiviral state, receptor signalling, cytokine interactions | RSAD2 (viperin) ($1.80 \times 10^{-140}$; 9.04).<br>IFIT5 (interferon induced protein with tetratricopeptide repeats 5) ($3.01 \times 10^{-119}$; 7.96). |
| M41 vs Beaudette | Downregulated | Cytokines, cytokine-receptor interactions | IL6 (interleukin 6) ($4.38 \times 10^{-4}$; –1.51).<br>IL8L1 (interleukin 8-like 1) ($1.38 \times 10^{-2}$;–1.44). |
| M41 vs Beaudette | Uregulated | * Heat shock family members | HSPA5 (heat shock 70kDa protein 5) ($2.28 \times 10^{-5}$; 1.74).<br>HSP90AA1(heat shock protein 90 alpha family class A member 1) ($4.38 \times 10^{-4}$; 1.44). |
| ***Translation*** | | | |
| Beaudette vs Mock | Downregulated | No obvious pathways identified (top two hits shown to right) | TIPARP (TCDD inducible poly(ADP-ribose) polymerase) ($8.42 \times 10^{-23}$; –4.32).<br>ADAMTS1 (ADAM metallopeptidase with thrombospondin type 1 motif 1) ($1.0 \times 10^{-12}$; –3.57). |
| M41 vs Mock | Downregulated | No obvious pathways identified (top two hits shown to right) | TIPARP (TCDD inducible poly(ADP-ribose) polymerase) ($8.42 \times 10^{-23}$; –4.32).<br>PFKFB3 (6-phosphofructo-2-kinase/fructose-2,6-biphosphatase 3) ($2.47 \times 10^{-13}$; –3.49). |
| Beaudette vs Mock | Upregulated | Antiviral response, translation, 80S ribosome, RACK1 | OASL (2'-5'-oligoadenylate synthetase like) ($5.08 \times 10^{-6}$; 2.24).<br>RPSL37 (ribosomal protein L37) ($5.34 \times 10^{-05}$; 1.78). |
| M41 vs Mock | Upregulated | Antiviral response, 80S ribosome | OASL (2'-5'-oligoadenylate synthetase-like) ($1.16 \times 10^{-3}$; 1.79).<br>RPS8 (ribosomal protein S8) ($1.03 \times 10^{-2}$; 1.35). |
| M41 vs Beaudette | Downregulated | No pathways identified | No significant genes identified. |
| M41 vs Beaudette | Upregulated | No pathways identified | Only one significant gene identified, MYH15 (myosin heavy chain 15) (0.032; 1.77) |

851
852
853 *Only six of the top 100 DEGs were significant in this category (see Supplementary Data S3).
854

855

856

857

858

**Figure 1**

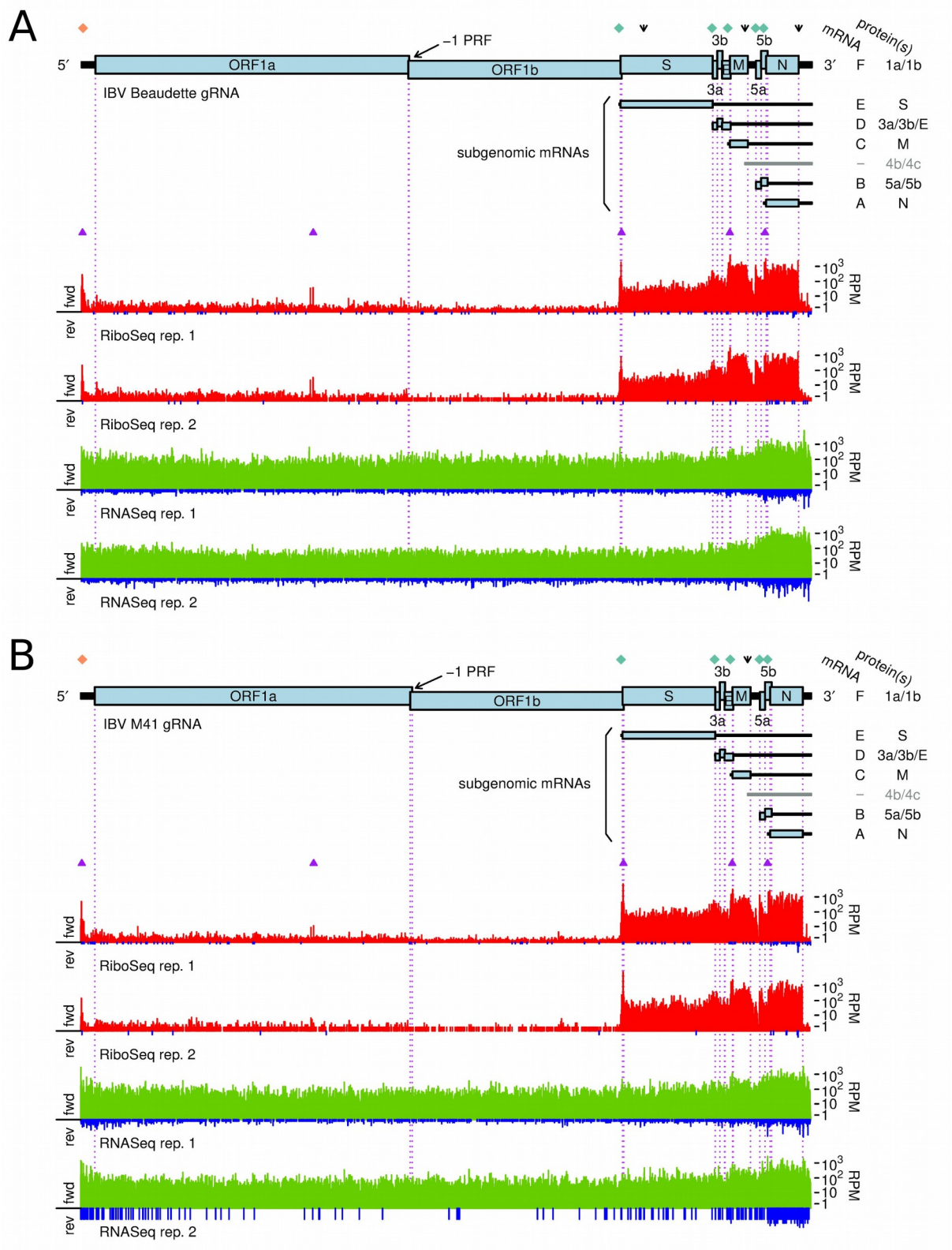

**Figure 2**

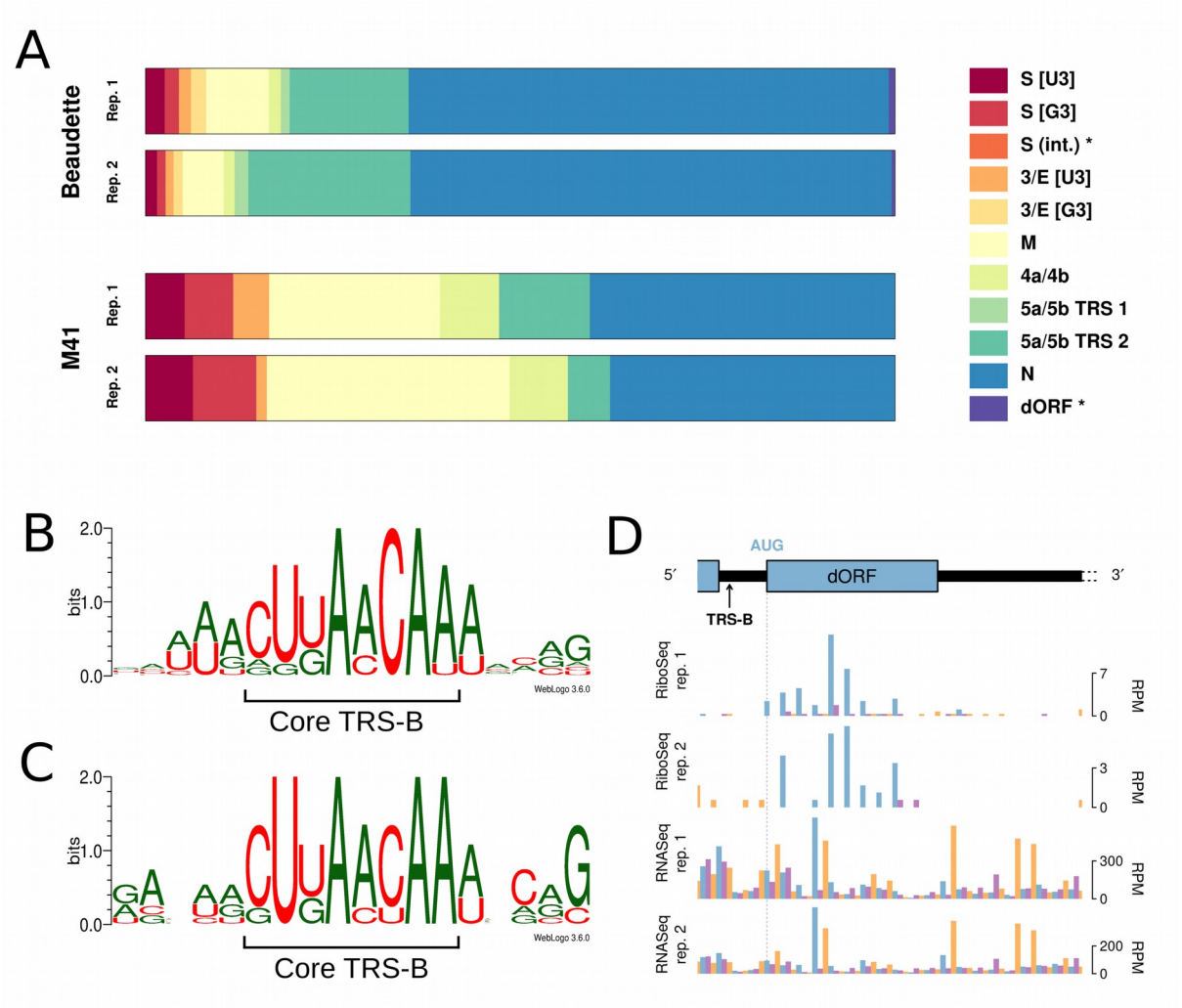

**Figure 3**

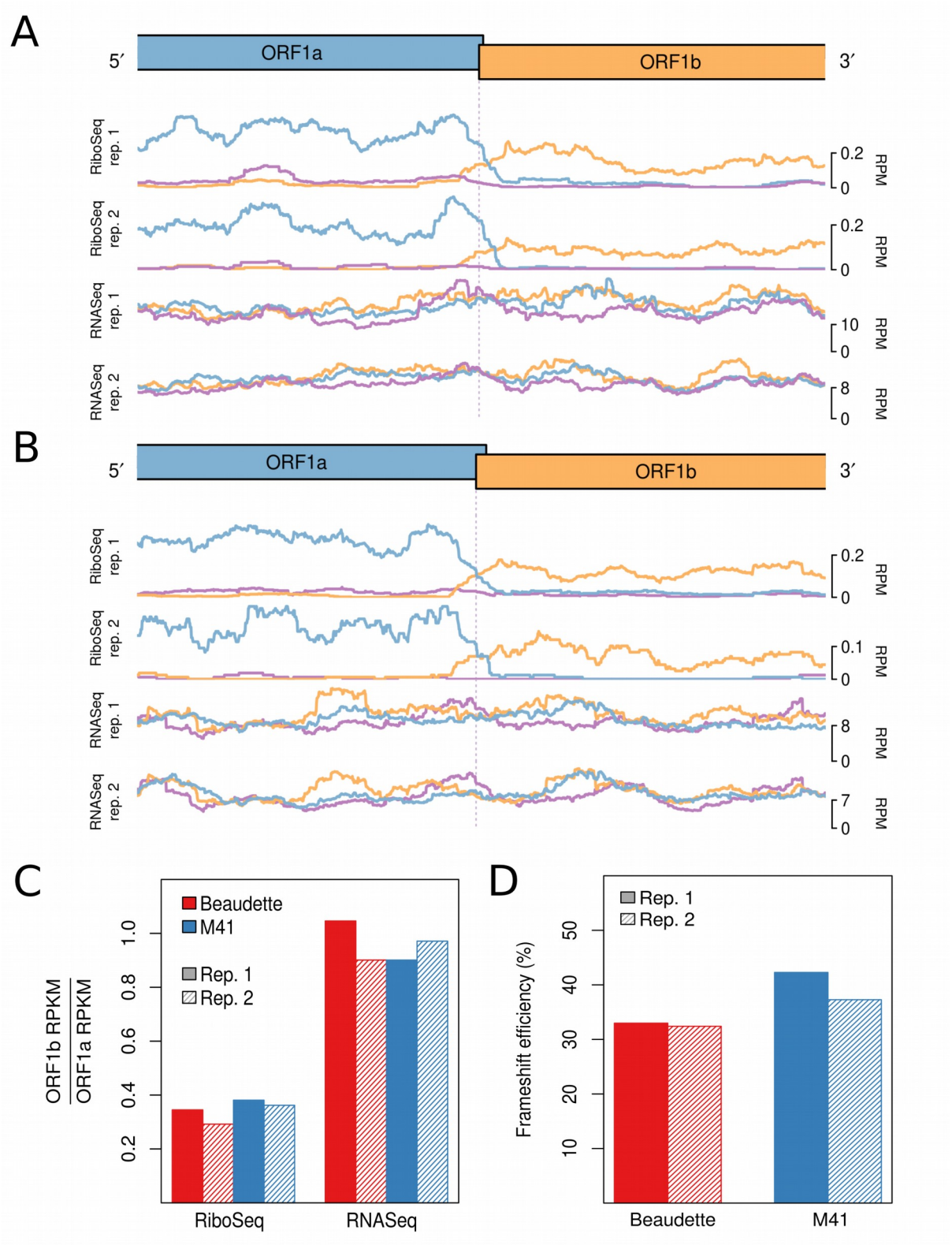

**Figure 4**

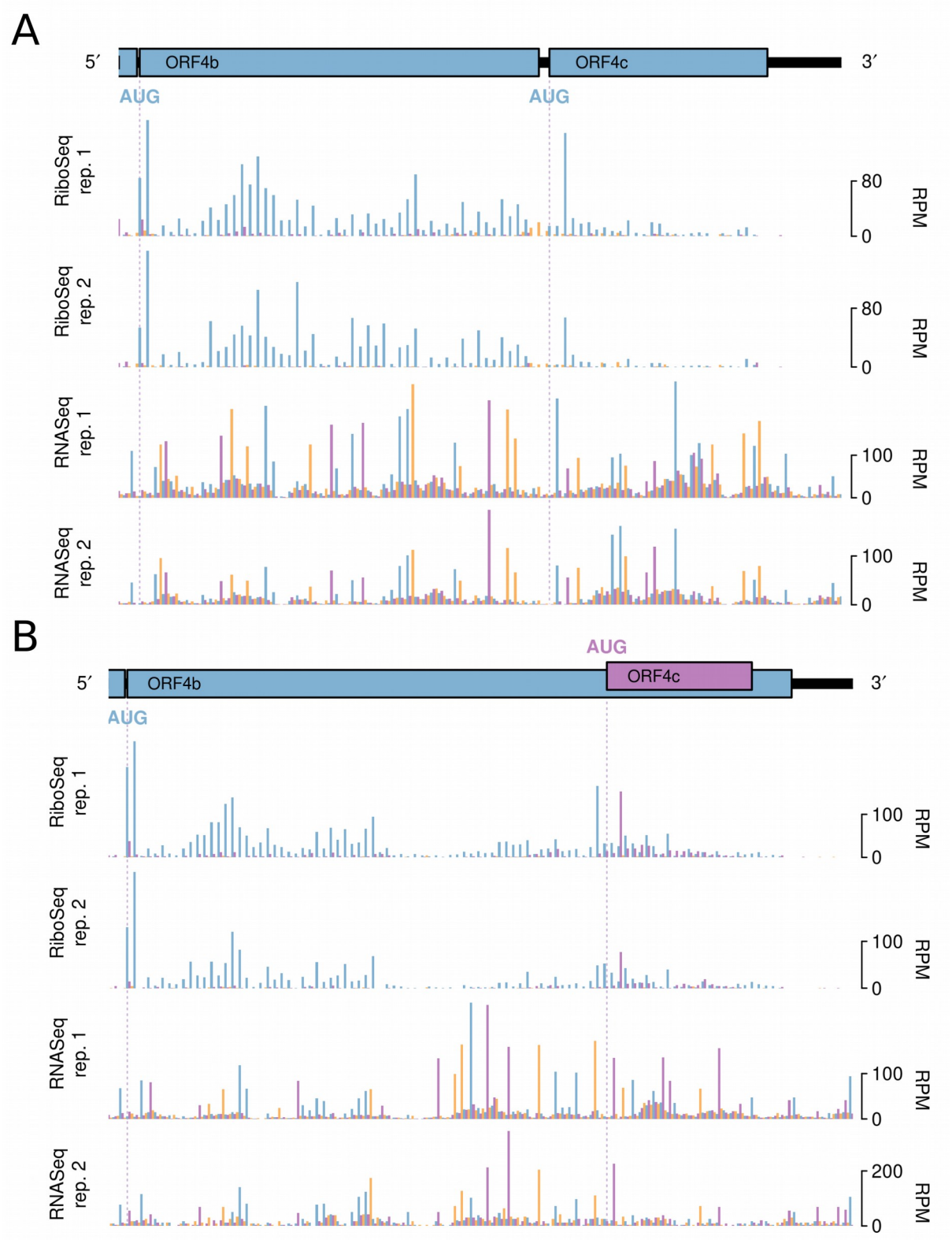

**Figure 5**

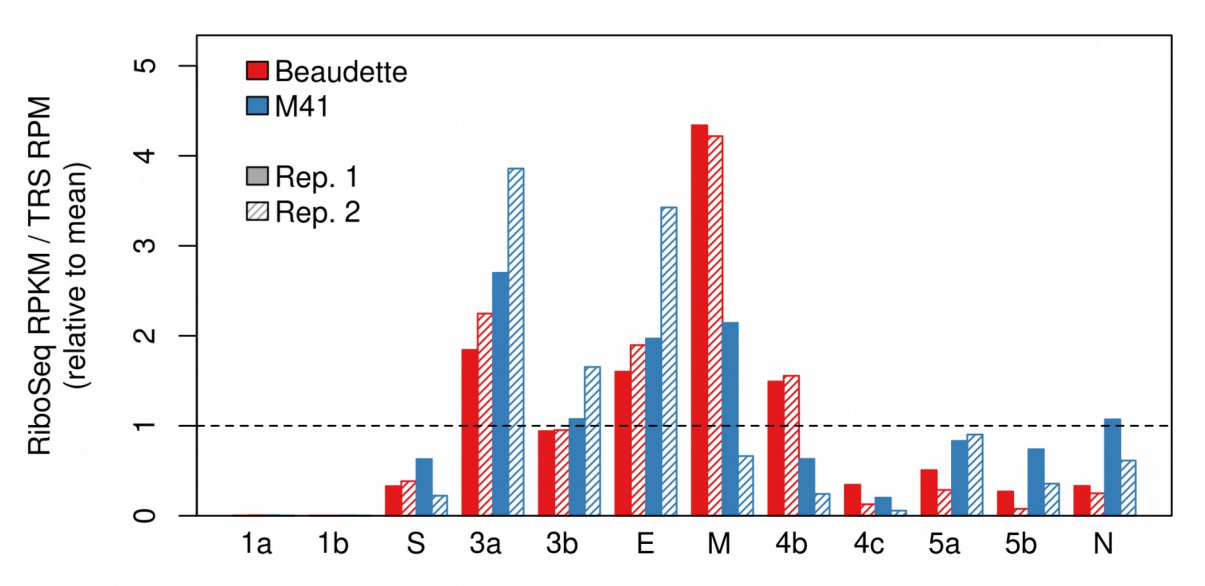


**Figure 6**

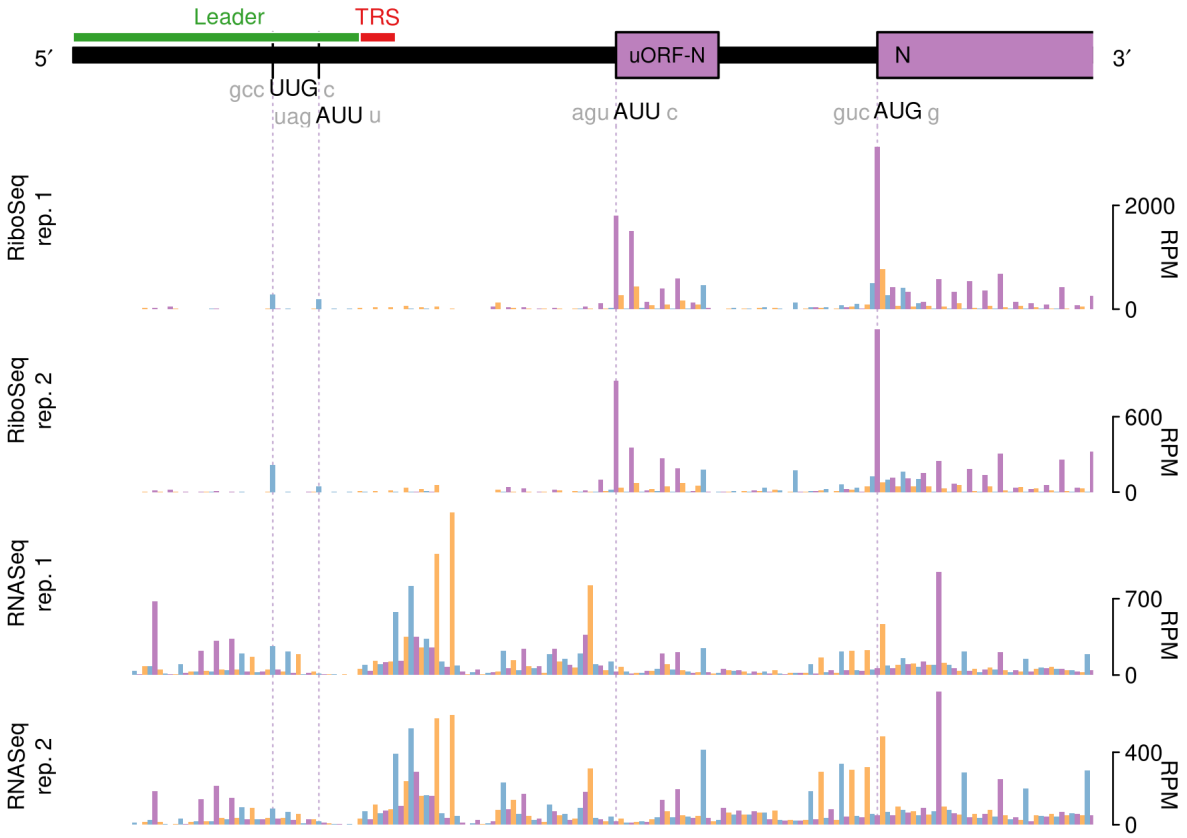

907
908
909
910
911 **Figure 7**
912

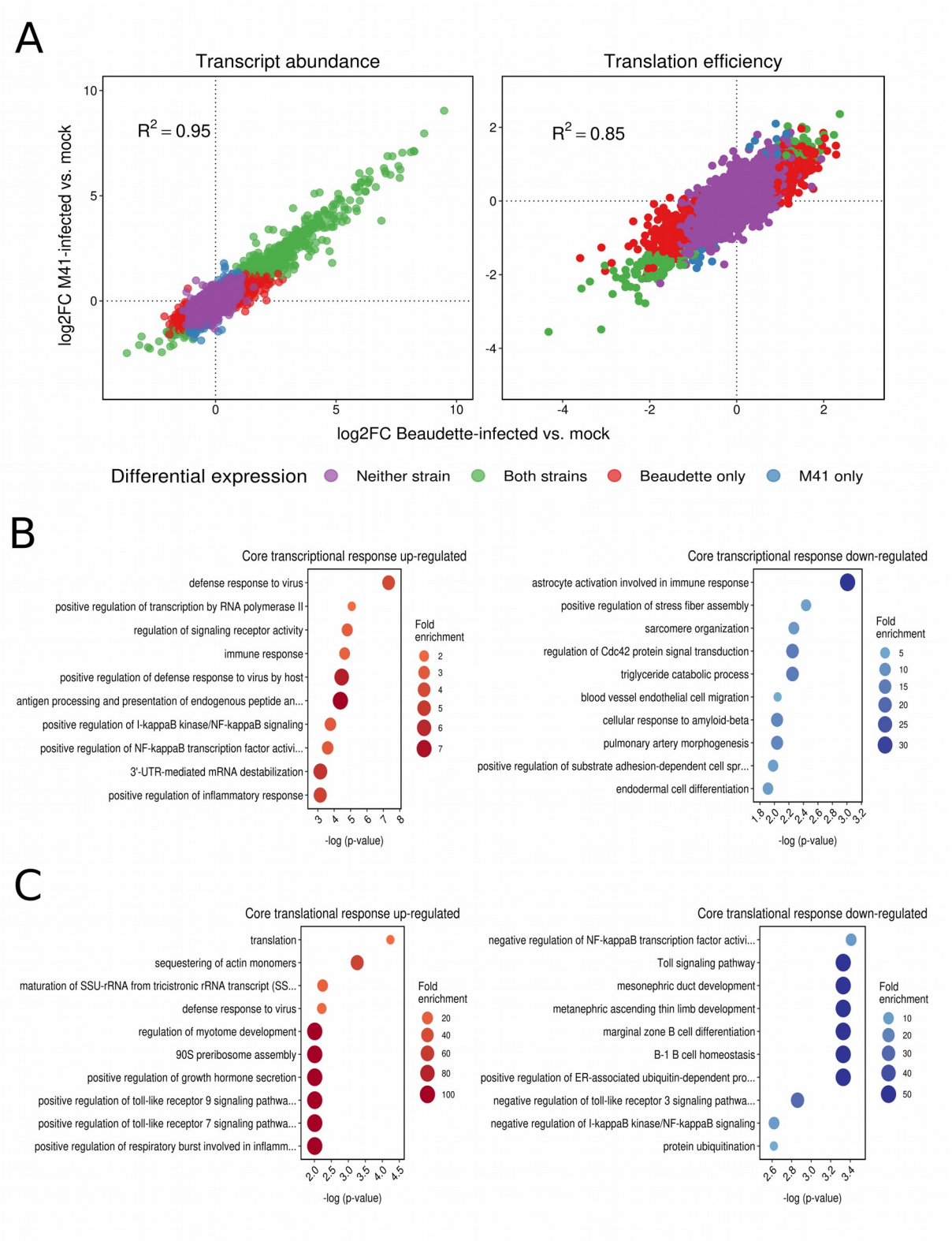

**Figure 8**

(A) M41 versus Mock downregulated

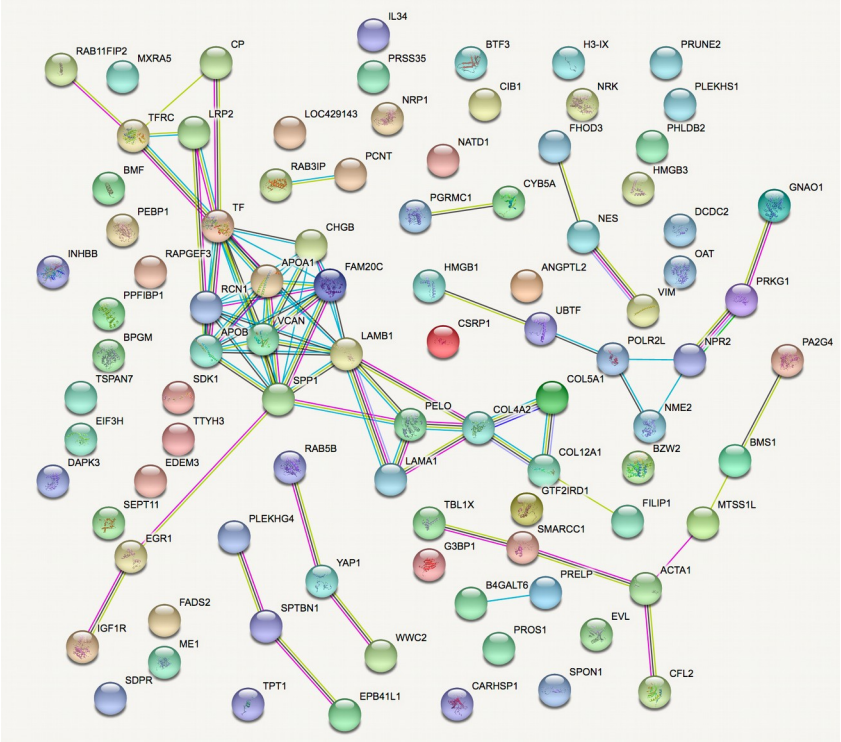


(B) M41 versus Mock upregulated

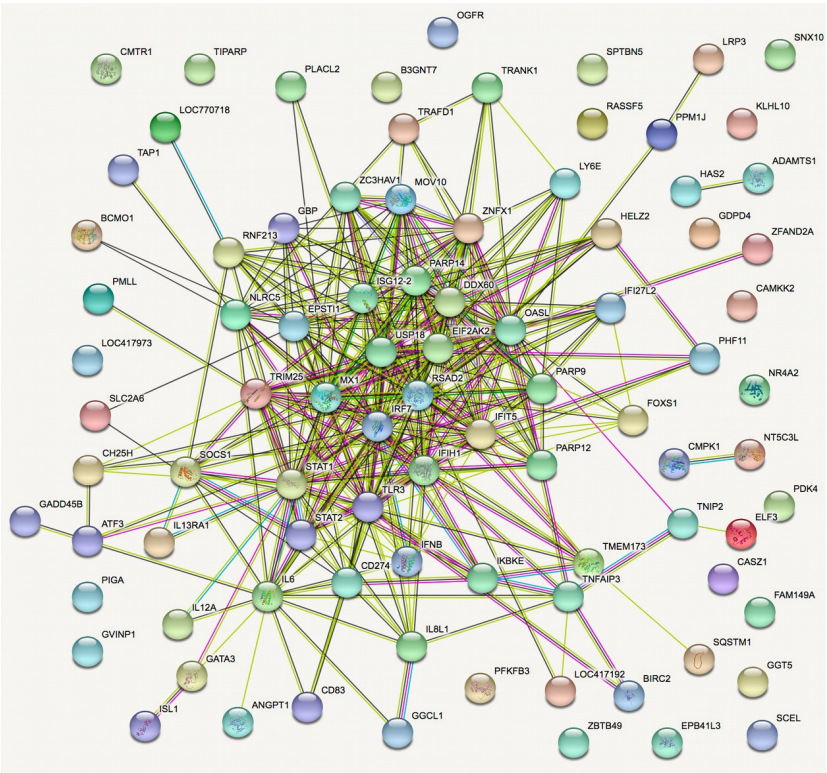

961
962
963
964

| Type | Condition | Total | De-duplicated | viral gRNA | | host mRNA |
|---|---|---|---|---|---|---|
| | | | | fwd | rev | |
| **Repeat 1** | | | | | | |
| RiboSeq | Beaudette-infected | 55,648,104 | 32,461,160 | 1,470,253 | 630 | 3,070,823 |
| | M41-infected | 47,459,412 | 24,416,659 | 1,838,613 | 792 | 4,193,904 |
| | Mock-infected | 46,640,167 | 26,170,072 | 399 | 1 | 9,400,391 |
| | | | | | | |
| RNASeq | Beaudette-infected | 27,720,370 | 12,171,506 | 2,365,784 | 4,842 | 882,421 |
| | M41-infected | 24,939,168 | 14,070,349 | 1,829,331 | 4,070 | 1,616,990 |
| | Mock-infected | 25,036,626 | 15,462,396 | 2,737 | 9 | 2,037,543 |
| | | | | | | |
| **Repeat 2** | | | | | | |
| RiboSeq | Beaudette-infected | 55,392,595 | 30,089,677 | 778,394 | 191 | 3,017,330 |
| | M41-infected | 51,319,886 | 27,664,513 | 540,016 | 63 | 1,978,766 |
| | Mock-infected | 56,813,327 | 26,535,892 | 159 | 1 | 3,413,589 |
| | | | | | | |
| RNASeq | Beaudette-infected | 26,792,717 | 15,637,095 | 2,606,240 | 8,245 | 1,840,748 |
| | M41-infected | 46,163,533 | 2,680,836 | 106,741 | 388 | 127,579 |
| | Mock-infected | 26,095,361 | 15,802,166 | 4,589 | 8 | 1,920,949 |
| | | | | | | |

**Table S1.** Library composition statistics: table of read counts per library. Random 7nt sequences were added to the ends of both 5′ and 3′ adaptors during library preparation to facilitate the removal of duplicate reads introduced during PCR. All libraries were de-duplicated following the removal of the adaptor sequences, as described in the Materials and Methods section. Numbers of reads mapped to the forward (fwd) and reverse (rev) strands of the viral gRNA are shown separately in each case; only forward strand-mapping reads are included in the host mRNA counts.

| TRS | Genomic TRS sequence | No. reads rep. 1 | No. reads rep. 2 | % rep. 1 | % rep. 2 |
|---|---|---|---|---|---|
| S [U3] | AAAA**CU**G**AACAA**AAGA | 176 | 158 | 2.58 | 1.53 |
| S [G3] | AAAA**CU**G**AACAA**AAGA | 129 | 120 | 1.89 | 1.16 |
| S (int.) | CAAA**CUUA**C**CAA**ACAA | 15 | 12 | 0.22 | 0.12 |
| 3/E [U3] | GUAA**CU**G**AACAA**UACA | 93 | 97 | 1.36 | 0.94 |
| 3/E [G3] | GUAA**CU**G**AACAA**UACA | 140 | 125 | 2.05 | 1.21 |
| M | AAAA**CUUAACAA**UCCG | 571 | 569 | 8.36 | 5.50 |
| 4a/4b | ACUGG**U**G**A**C**CAA**AGCG | 109 | 147 | 1.60 | 1.42 |
| 5_1 | UUUA**CUUAACAA**AAAC | 81 | 189 | 1.19 | 1.83 |
| 5_2 | AAAA**CUUAACAA**AUAC | 1,085 | 2,237 | 15.88 | 21.63 |
| N | CUUU**CUUAACAA**AGCA | 4,376 | 6,643 | 64.05 | 64.24 |
| dORF | UUUGAG**UAACAU**AAUG | 57 | 44 | 0.83 | 0.43 |

**Table S2. (A)** Chimeric TRS-spanning reads identified in IBV Beaudette samples. Residues matching the leader TRS (TRS-L) are shown in bold.

| TRS | Genomic TRS sequence | No. reads rep. 1 | No. reads rep. 2 | % rep. 1 | % rep. 2 |
|---|---|---|---|---|---|
| S [U3] | AAAA**CU**G**AACAA**AAGA | 200 | 9 | 5.21 | 6.34 |
| S [G3] | AAAA**CU**G**AACAA**AAGA | 250 | 12 | 6.51 | 8.45 |
| S (int.) | CAAA**CUUA**C**CAA**ACAC | 1 | 0 | 0.03 | 0 |
| 3/E [U3] | GUAA**CUUAACAA**UACA | 182 | 2 | 4.74 | 1.41 |
| 3/E [G3] | GUAA**CUUAACAA**UACA | 0 | 0 | 0 | 0 |
| M | AAAA**CUUAACAA**UCCG | 877 | 46 | 22.83 | 32.39 |
| 4a/4b | ACUGG**U**G**A**C**CAA**AGCG | 303 | 11 | 7.89 | 7.75 |
| 5_2 | AGCG**CUUAA**U**AA**AUAC | 464 | 8 | 12.08 | 5.63 |
| N | CUUU**CUUAACAA**AGCA | 1565 | 54 | 40.74 | 38.03 |

**Table S2. (B)** Chimeric TRS-spanning reads identified in IBV M41 samples. Residues matching the leader TRS (TRS-L) are shown in bold.

997

| GO.ID | Term | Annotated | Significant | Expected | P-value |
|---|---|---|---|---|---|
| GO:0010469 | regulation of signaling receptor activity | 53 | 7 | 0.58 | $1.2 \times 10^{-6}$ |
| GO:0048661 | positive regulation of smooth muscle cell proliferation | 18 | 5 | 0.2 | $3.5 \times 10^{-5}$ |
| GO:2000352 | negative regulation of endothelial cell apoptotic process | 9 | 3 | 0.1 | $9.7 \times 10^{-5}$ |
| GO:0060585 | positive regulation of prostaglandin-endoperoxide synthase | 2 | 2 | 0.02 | $1.2 \times 10^{-4}$ |
| GO:0033141 | positive regulation of peptidyl-serine phosphorylation of ST... | 2 | 2 | 0.02 | $1.2 \times 10^{-4}$ |
| GO:0014826 | vein smooth muscle contraction | 2 | 2 | 0.02 | $1.2 \times 10^{-4}$ |
| GO:1900625 | positive regulation of monocyte aggregation | 2 | 2 | 0.02 | $1.2 \times 10^{-4}$ |
| GO:0014824 | artery smooth muscle contraction | 3 | 2 | 0.03 | $3.5 \times 10^{-4}$ |
| GO:0003100 | regulation of systemic arterial blood pressure by endothelin | 3 | 2 | 0.03 | $3.5 \times 10^{-4}$ |
| GO:1901842 | negative regulation of high voltage-gated calcium channel ac... | 3 | 2 | 0.03 | $3.5 \times 10^{-4}$ |
| GO:0006955 | immune response | 244 | 12 | 2.66 | $5.9 \times 10^{-4}$ |
| GO:1904754 | positive regulation of vascular associated smooth muscle cel... | 4 | 2 | 0.04 | $6.9 \times 10^{-4}$ |
| GO:0071356 | cellular response to tumor necrosis factor | 40 | 4 | 0.44 | $8.4 \times 10^{-4}$ |
| GO:0043154 | negative regulation of cysteine-type endopeptidase activity ... | 18 | 3 | 0.2 | $8.8 \times 10^{-4}$ |
| GO:0001516 | prostaglandin biosynthetic process | 8 | 3 | 0.09 | $1.09 \times 10^{-3}$ |
| GO:0071498 | cellular response to fluid shear stress | 8 | 3 | 0.09 | $1.09 \times 10^{-3}$ |
| GO:0002931 | response to ischemia | 5 | 2 | 0.05 | $1.14 \times 10^{-3}$ |
| GO:0090051 | negative regulation of cell migration involved in sprouting ... | 5 | 2 | 0.05 | $1.14 \times 10^{-3}$ |
| GO:0019229 | regulation of vasoconstriction | 5 | 2 | 0.05 | $1.14 \times 10^{-3}$ |
| GO:0070373 | negative regulation of ERK1 and ERK2 cascade | 22 | 3 | 0.24 | $1.16 \times 10^{-3}$ |

998

999 **Table S3.** Top 20 most significantly enriched GO terms among genes which are down-regulated in
1000 IBV M41-infected cells relative to IBV Beaudette-infected cells. Column “Annotated” shows the
1001 total number of genes in the data set which are members of that GO term; “Significant” shows the

number that are significantly differentially expressed; and “Expected” shows the proportion of genes that would be expected to occur in a random sample.

1008

| GO.ID | Term | Annotated | Significant | Expected | P-value |
|---|---|---|---|---|---|
| GO:0042026 | protein refolding | 7 | 2 | 0.01 | $4.4 \times 10^{-5}$ |
| GO:0051085 | chaperone cofactor-dependent protein refolding | 9 | 2 | 0.01 | $7.6 \times 10^{-5}$ |
| GO:0034605 | cellular response to heat | 17 | 2 | 0.03 | $2.9 \times 10^{-4}$ |
| GO:0090074 | negative regulation of protein homodimerization activity | 1 | 1 | 0 | $1.6 \times 10^{-3}$ |
| GO:1905719 | protein localization to perinuclear region of cytoplasm | 1 | 1 | 0 | $1.6 \times 10^{-3}$ |
| GO:1903895 | negative regulation of IRE1-mediated unfolded protein respon... | 1 | 1 | 0 | $1.6 \times 10^{-3}$ |
| GO:0070194 | synaptonemal complex disassembly | 1 | 1 | 0 | $1.6 \times 10^{-3}$ |
| GO:0006880 | intracellular sequestering of iron ion | 1 | 1 | 0 | $1.6 \times 10^{-3}$ |
| GO:0034620 | cellular response to unfolded protein | 36 | 3 | 0.06 | $2.5 \times 10^{-3}$ |
| GO:1902949 | positive regulation of tau-protein kinase activity | 2 | 1 | 0 | $3.2 \times 10^{-3}$ |
| GO:1903071 | positive regulation of ER-associated ubiquitin-dependent pro... | 2 | 1 | 0 | $3.19 \times 10^{-3}$ |
| GO:1901896 | positive regulation of calcium-transporting ATPase activity | 2 | 1 | 0 | $3.19 \times 10^{-3}$ |
| GO:0090084 | negative regulation of inclusion body assembly | 3 | 1 | 0 | $4.78 \times 10^{-3}$ |
| GO:1905323 | telomerase holoenzyme complex assembly | 3 | 1 | 0 | $4.78 \times 10^{-3}$ |
| GO:0044130 | negative regulation of growth of symbiont in host | 3 | 1 | 0 | $4.78 \times 10^{-3}$ |
| GO:0007141 | male meiosis I | 3 | 1 | 0 | $4.78 \times 10^{-3}$ |
| GO:0031396 | regulation of protein ubiquitination | 73 | 2 | 0.12 | $5.31 \times 10^{-3}$ |
| GO:0035973 | aggrephagy | 4 | 1 | 0.01 | $6.38 \times 10^{-3}$ |
| GO:0061635 | regulation of protein complex stability | 4 | 1 | 0.01 | $6.38 \times 10^{-3}$ |
| GO:1900273 | positive regulation of long-term synaptic potentiation | 4 | 1 | 0.01 | $6.38 \times 10^{-3}$ |

**Table S4.** Top 20 most significantly enriched GO terms among genes which are up-regulated in IBV M41-infected cells relative to IBV Beaudette-infected cells. Column “Annotated” shows the total number of genes in the data set which are members of that GO term; “Significant” shows the number that are significantly differentially expressed; and “Expected” shows the proportion of genes that would be expected to occur in a random sample.

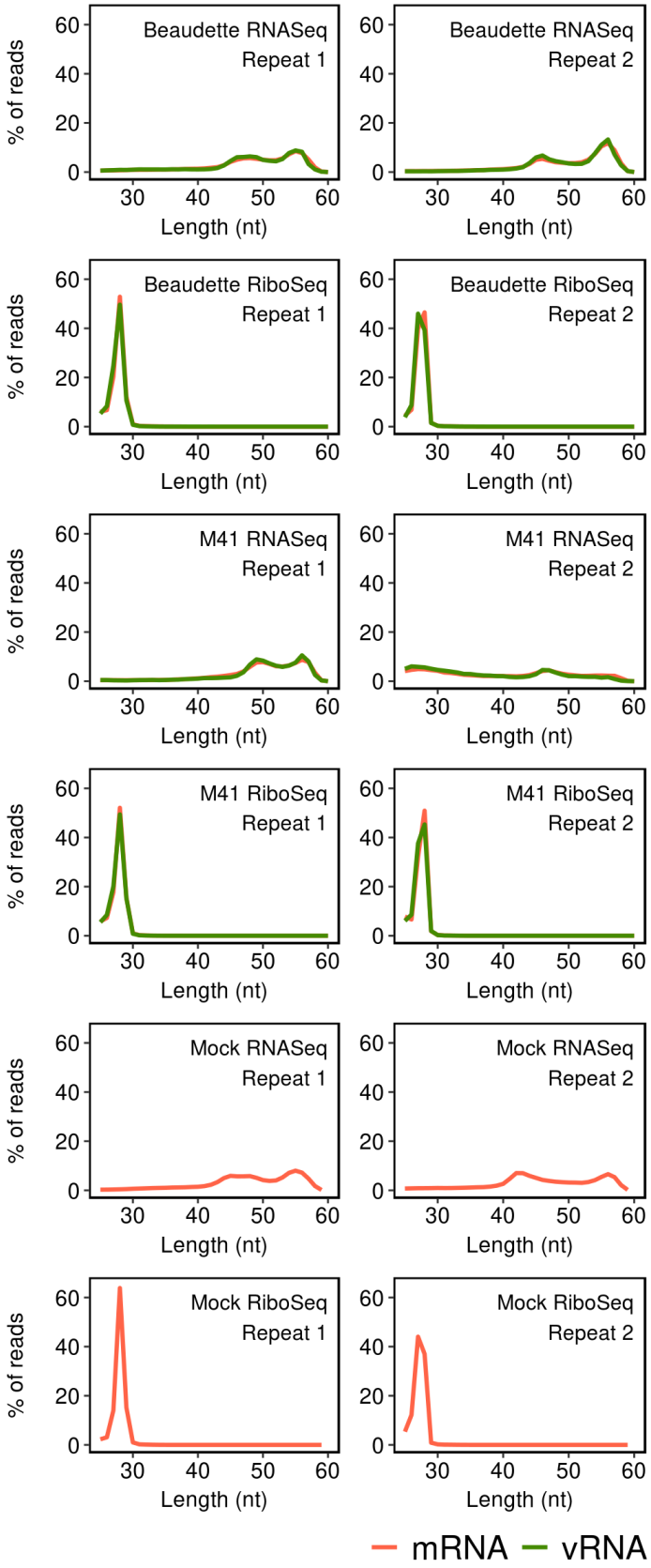


1020 **Figure S1.** Length distribution of reads mapped to the internal regions of protein-coding sequences
1021 on viral RNA (vRNA; green lines) and host mRNA (red lines).

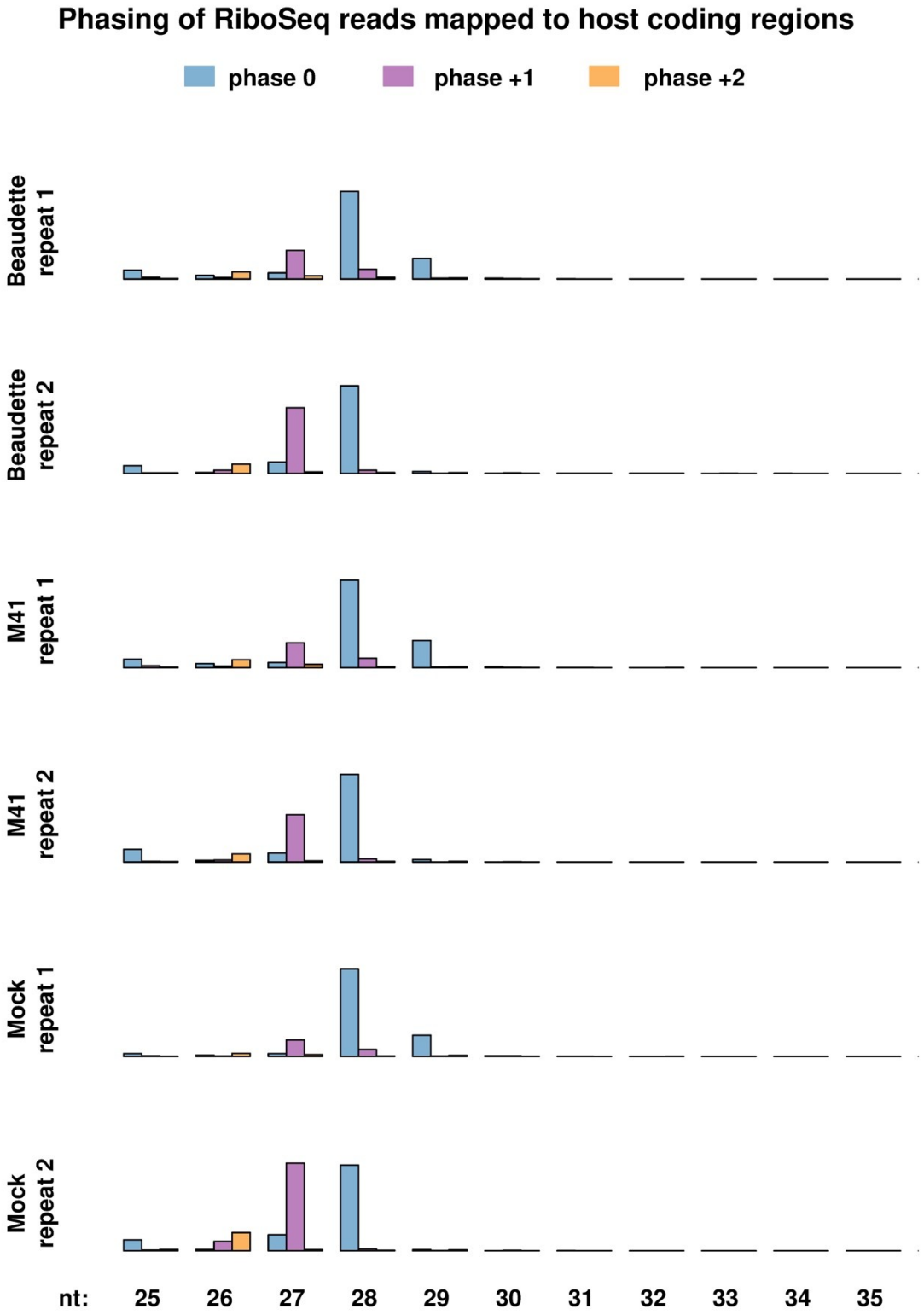


**Figure S2.** Phasing of RiboSeq reads mapped to the internal regions of protein-coding sequences in host mRNAs for different RPF lengths.

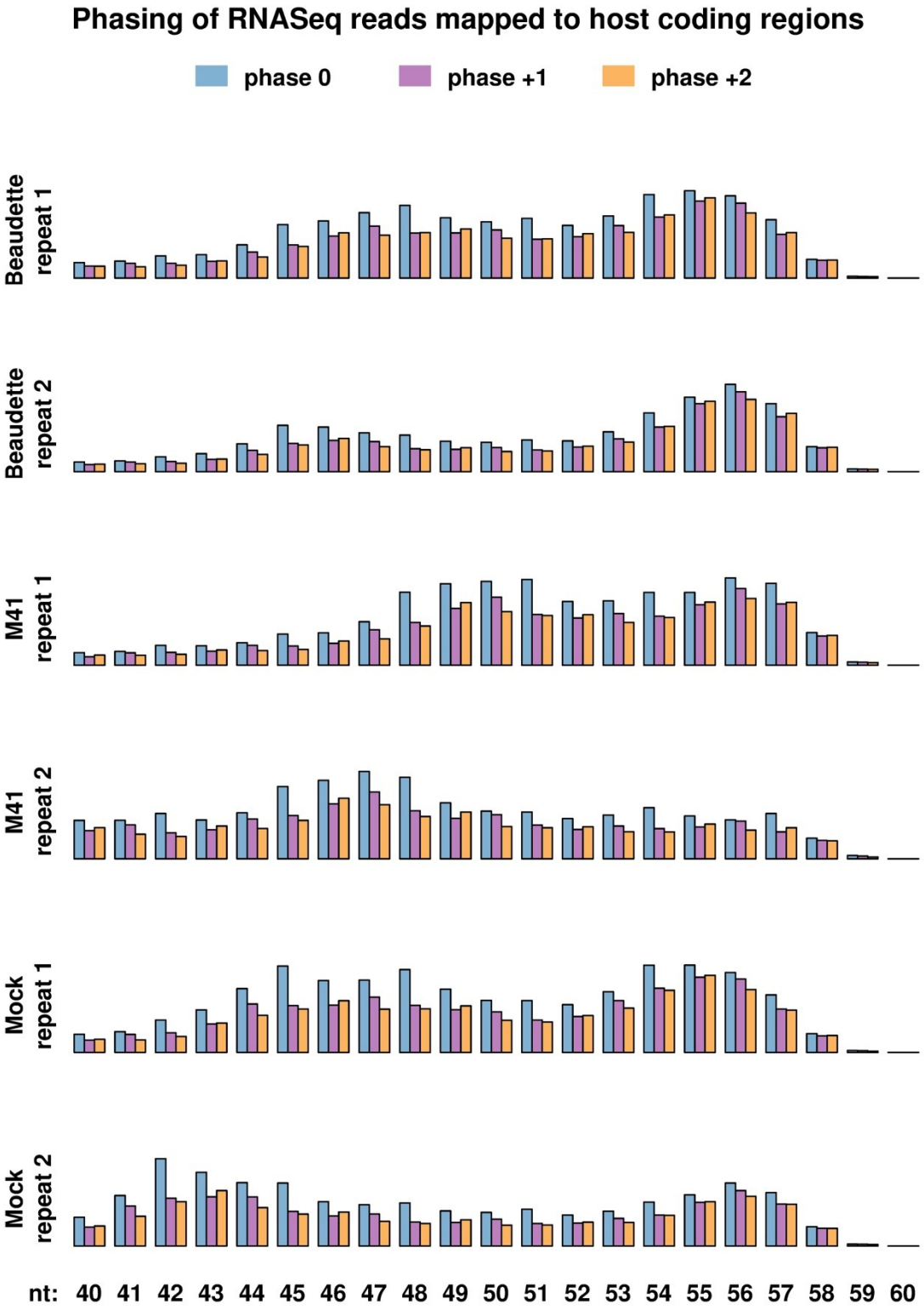


1025 **Figure S3.** Phasing of RNASeq reads mapped to the internal regions of protein coding sequences in
1026 host mRNAs. To aid visualisation, only reads between 40 nt and 60 nt in length are shown.
1027

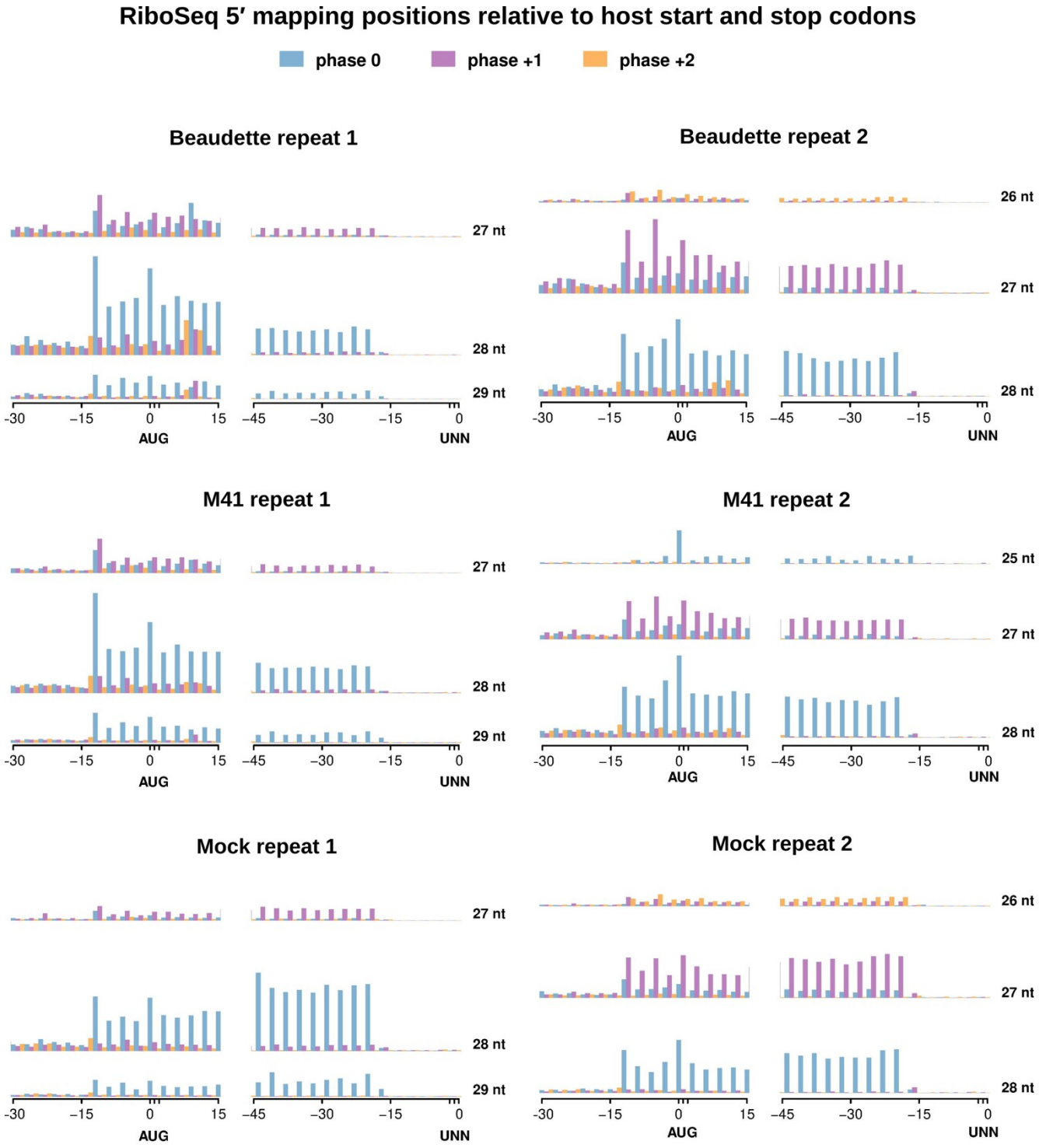


**Figure S4.** Histograms of 5′ mapping positions of RiboSeq reads relative to host mRNA start (AUG) and stop (UNN) codons. Positions indicated are relative to the first nt of the AUG codon (left) and the last nt of the UNN codon (right). The three most abundant read lengths are plotted for each library.

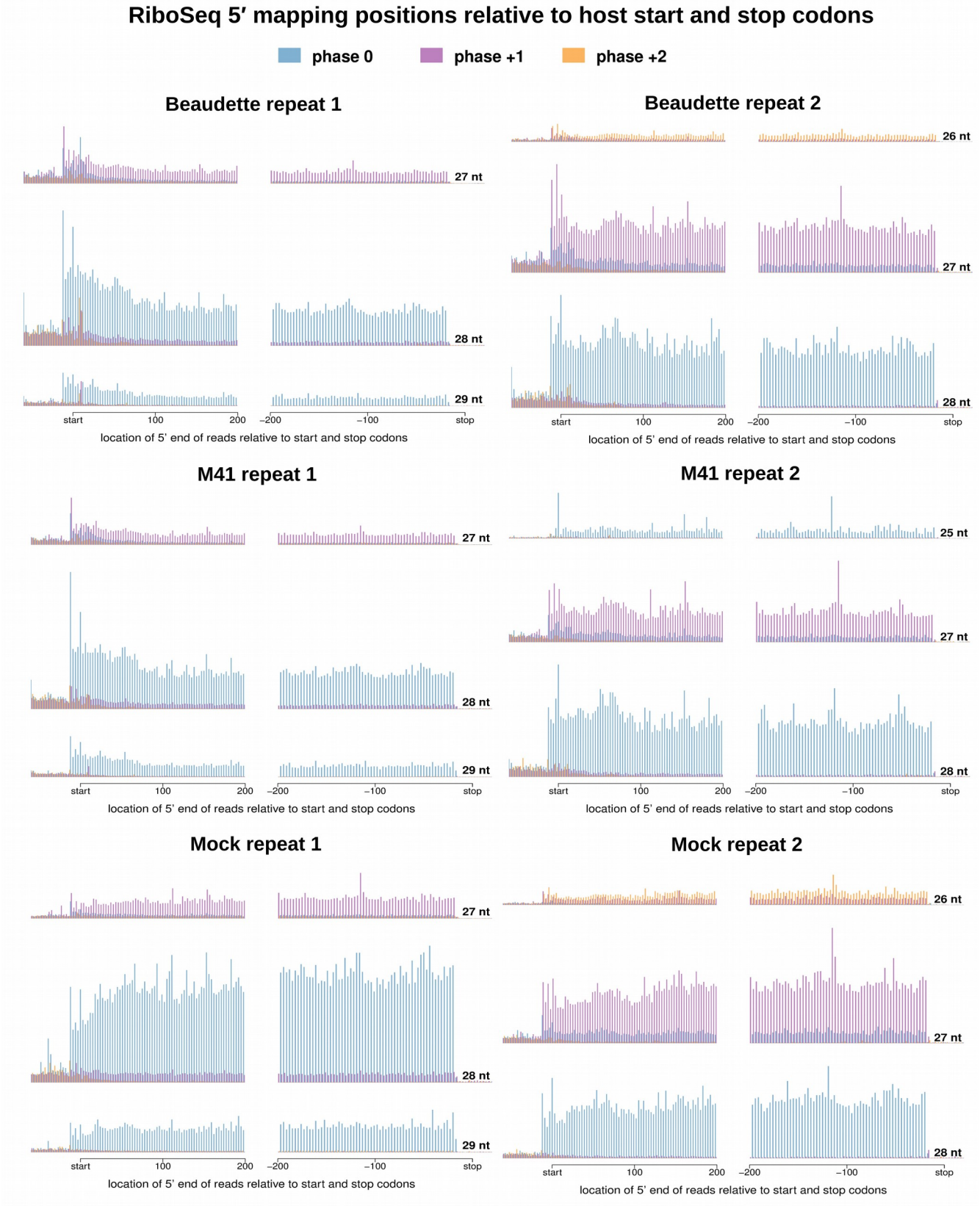


1037 **Figure S5.** Histograms of 5′ mapping positions of RiboSeq reads relative to host mRNA start and
1038 stop codons. The three most abundant read lengths are plotted for each library.

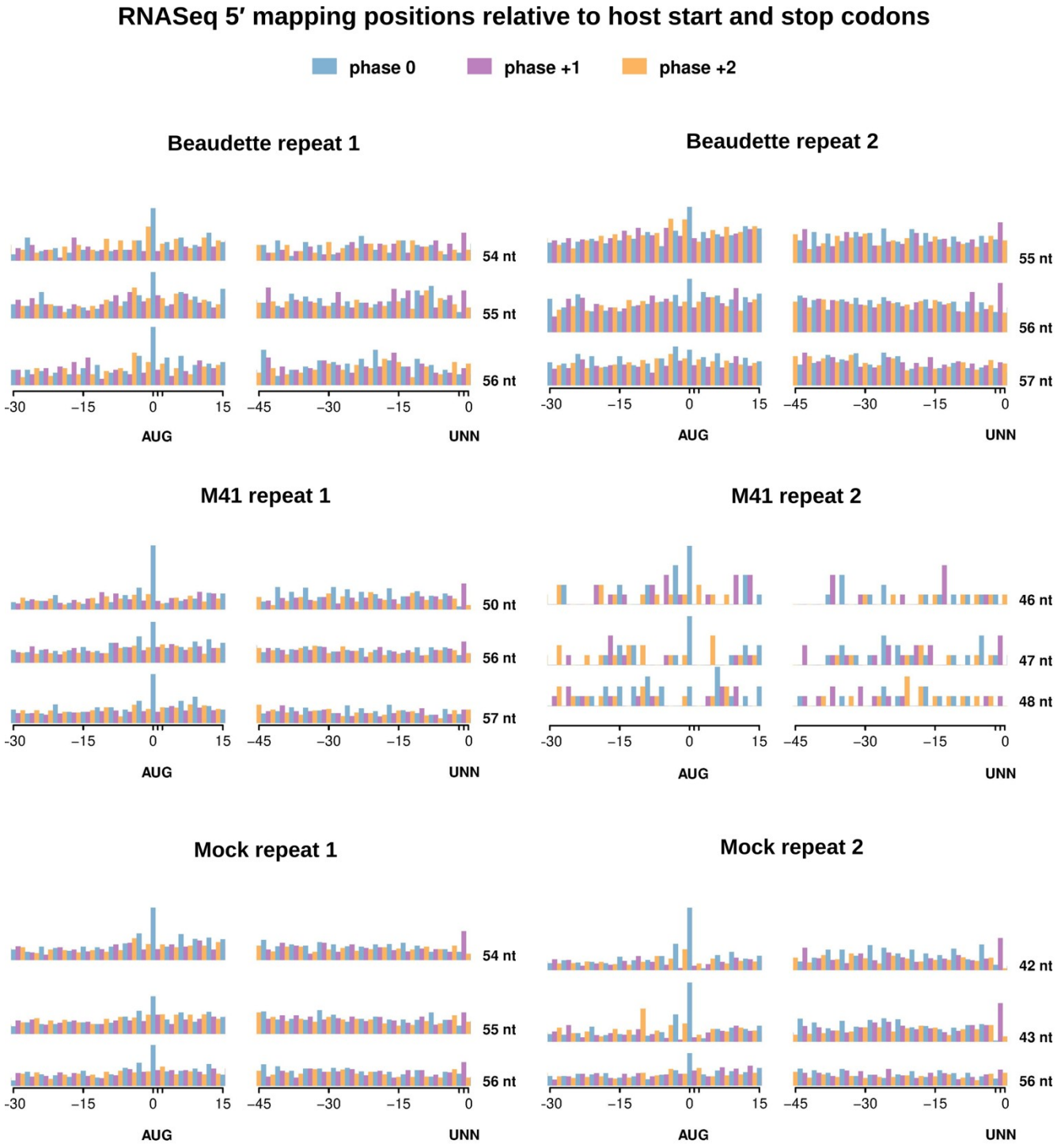


**Figure S6.** Histograms of 5′ mapping positions of RNASeq reads relative to host mRNA start (AUG) and stop (UNN) codons. Positions indicated are relative to the first nt of the AUG codon (left) and the last nt of the UNN codon (right). The three most abundant read lengths are plotted for each library.

1046

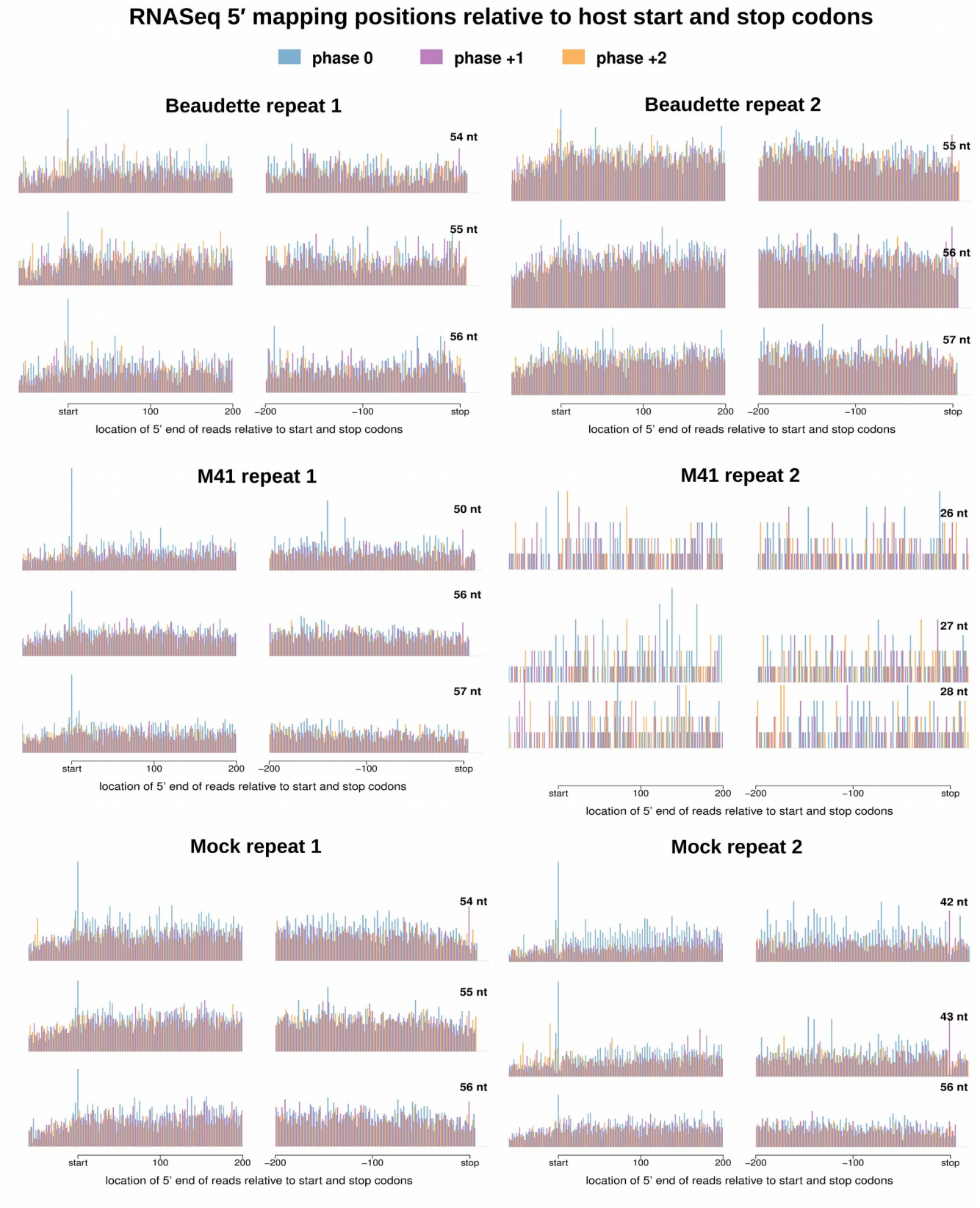


1048 **Figure S7.** Histograms of 5′ mapping positions of RNASeq reads relative to host mRNA start and
1049 stop codons. The three most abundant read lengths are plotted for each library**.**

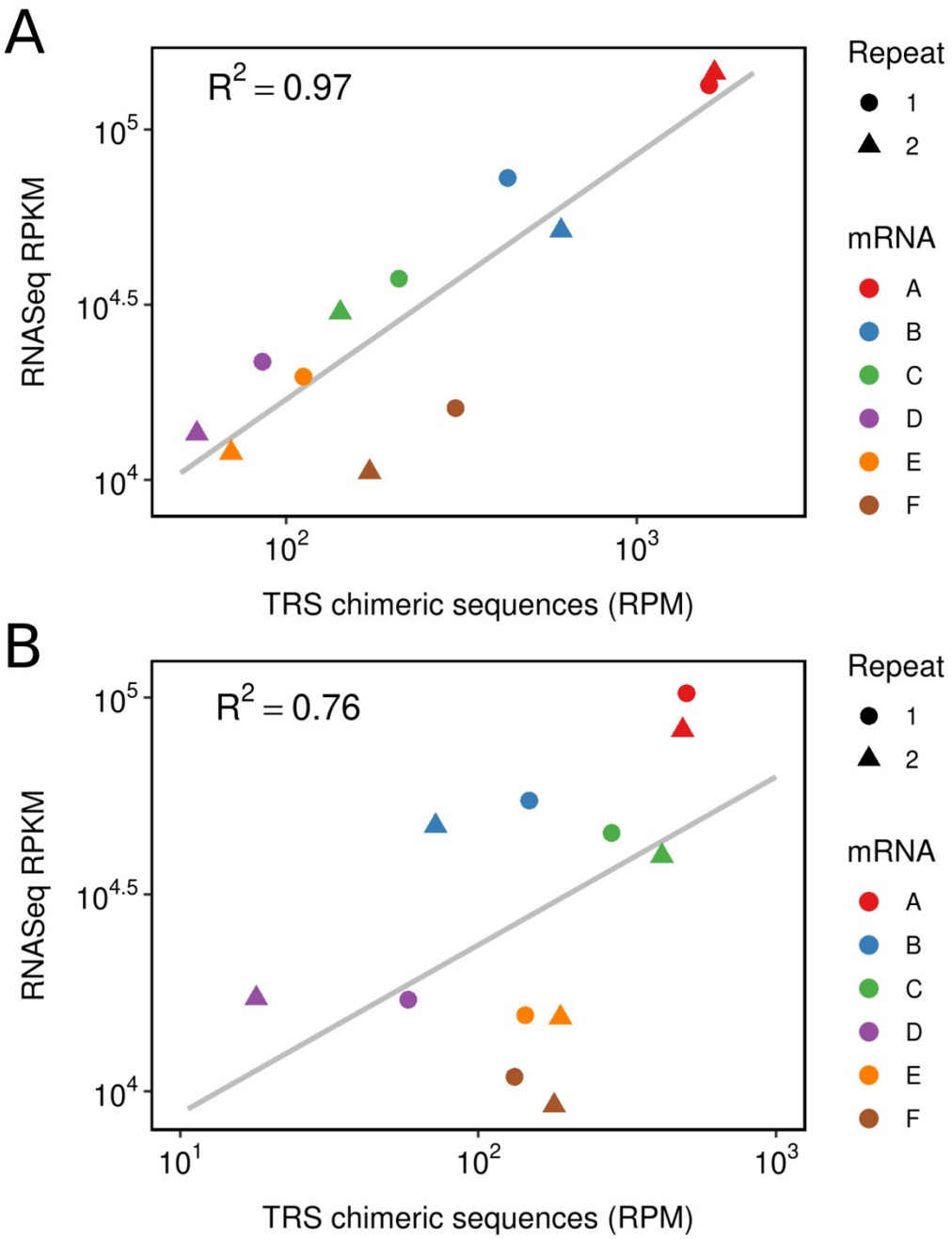


**Figure S8.** Relative abundances of sgmRNAs (mRNA A to E) and gRNA (mRNA F) for **(A)** IBV Beaudette and **(B)** IBV M41, as measured by decumulating RNASeq coverage (see Methods) or by counting chimeric reads spanning the TRS sequence. RNASeq densities are expressed as reads per kilobase per million mapped reads (RPKM), and chimeric TRS-spanning reads are expressed as reads per million mapped reads (RPM).

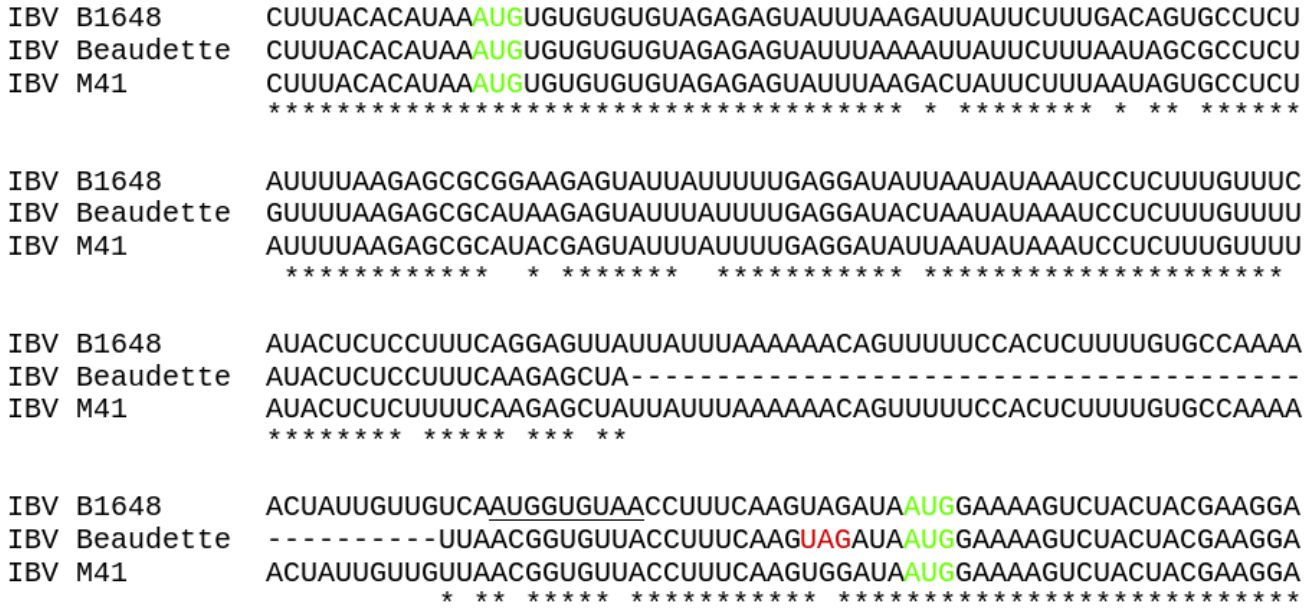


**Figure S9.** Alignment of IBV sequences, showing the positions of the ORF4b and ORF4c initiation codons (green). A 49-nt deletion in the Beaudette strain prematurely truncates the ORF4b gene by bringing a UAG codon (red) in frame. Note the absence of AUG codons between the starts of ORF4b and ORF4c in both IBV Beaudette and IBV M41, consistent with a leaky scanning mechanism for 4c expression. Conversely, the genome of the Belgian nephropathogenic strain B1648 contains an intervening AUG (underlined; 2-codon ORF) towards the 3′ end of ORF4b.

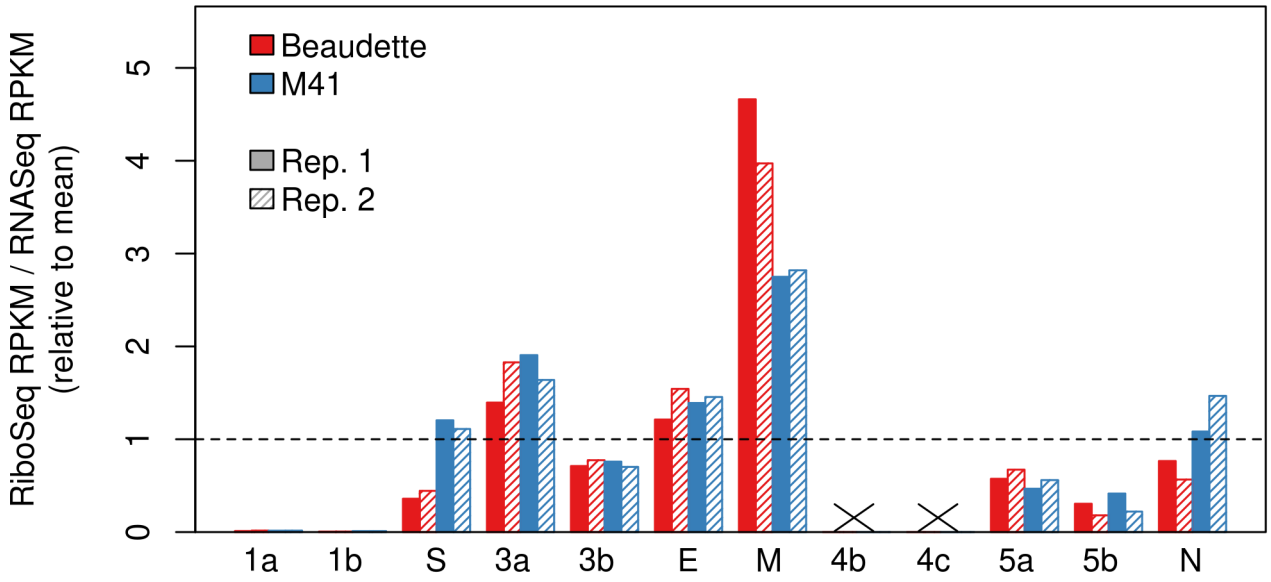


**Figure S10.** Viral gene translation efficiency values calculated using decumulated RNASeq reads (expressed as reads per kilobase per million mapped reads [RPKM]). The ratio of RiboSeq RPKM to RNASeq RPKM is plotted relative to the mean across all samples.

**Figure S11.** STRING analysis of the relationship between differentially expressed genes in comparisons of IBV Beaudette, IBV M41 and mock-infected chick kidney cells (**panels A to I**). The network nodes represent the proteins encoded by the differentially expressed genes. Seven different coloured lines link a number of nodes and represent seven types of evidence used in predicting associations. A red line indicates the presence of fusion evidence; a green line represents neighborhood evidence; a blue line represents co-ocurrence evidence; a purple line represents experimental evidence; a yellow line represents text-mining evidence; a light blue line represents database evidence; and a black line represents co-expression evidence.

(**A**) Beaudette vs Mock downregulated transcripts

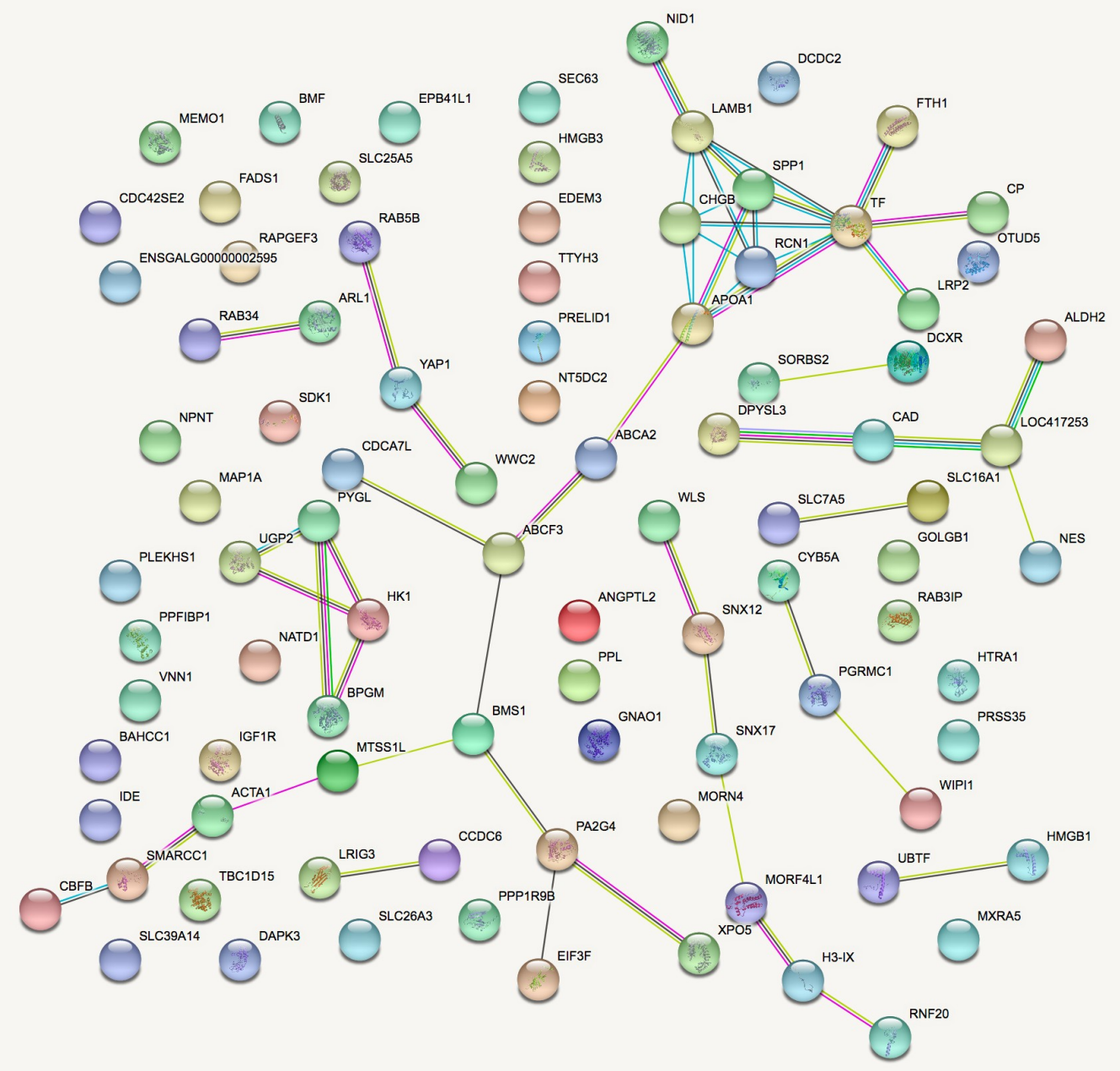

(**B**) M41 vs Mock downregulated transcripts

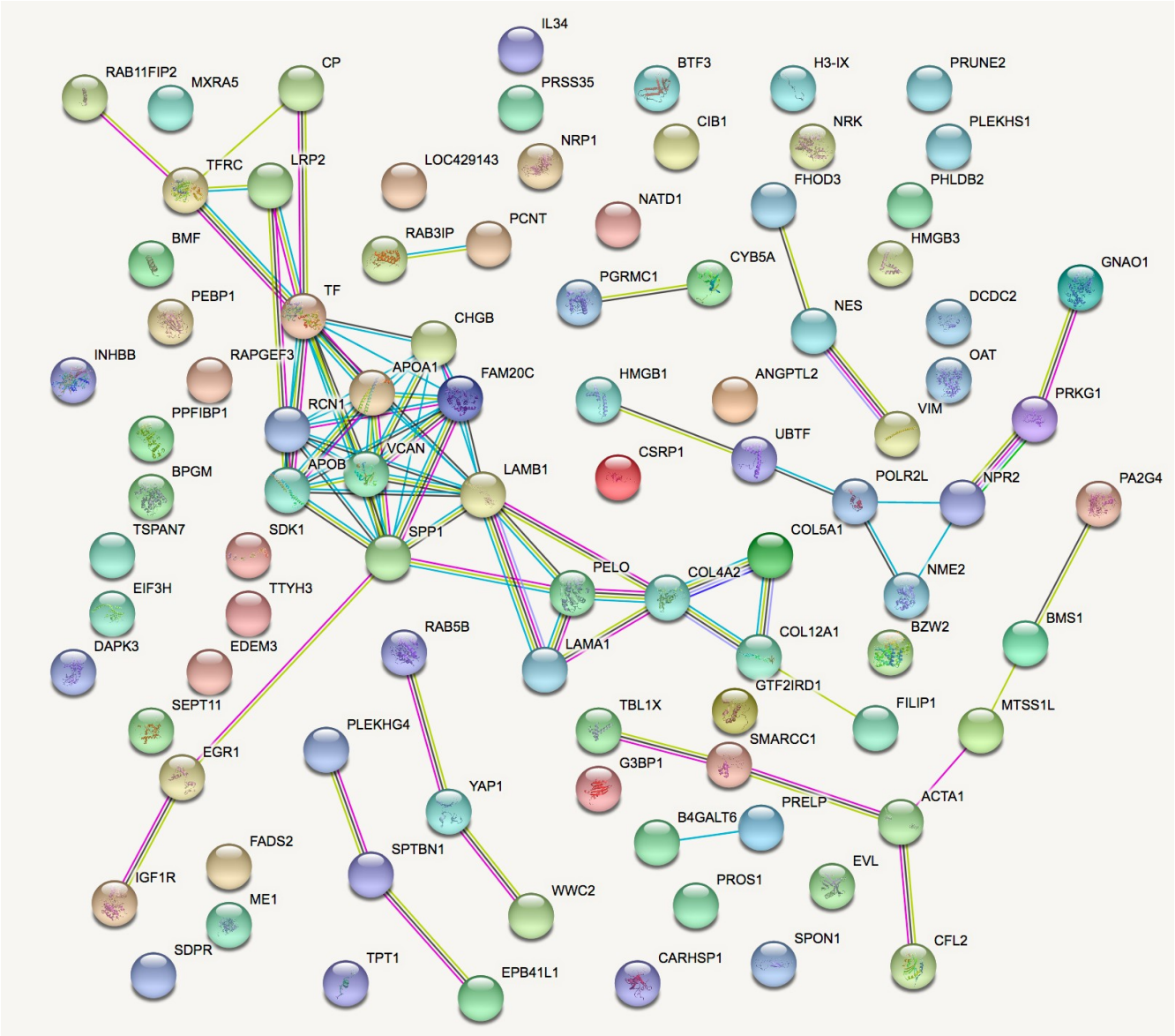

(**C**) Beaudette vs Mock upregulated transcripts

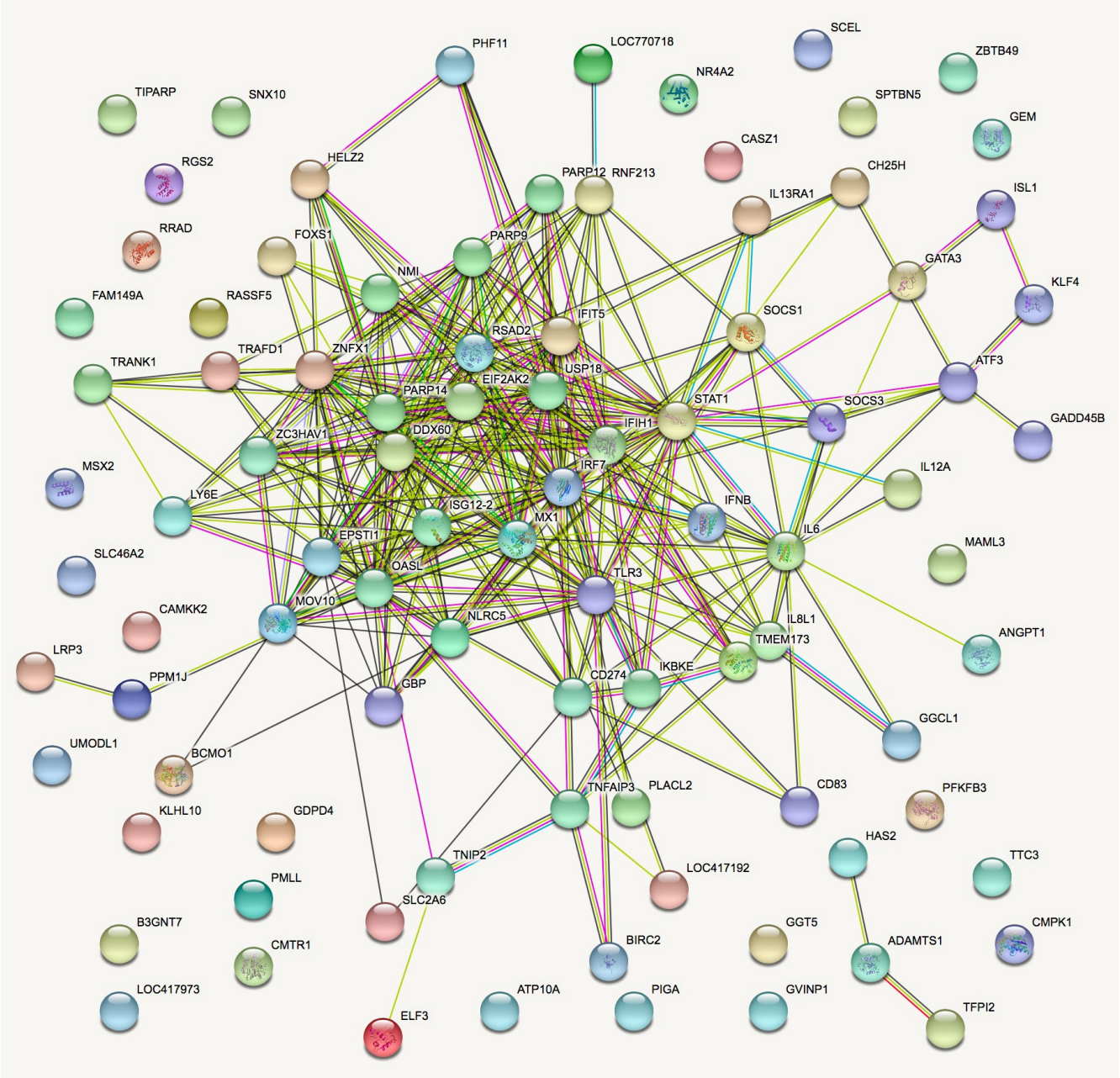

(**D**) M41 vs Mock upregulated transcripts

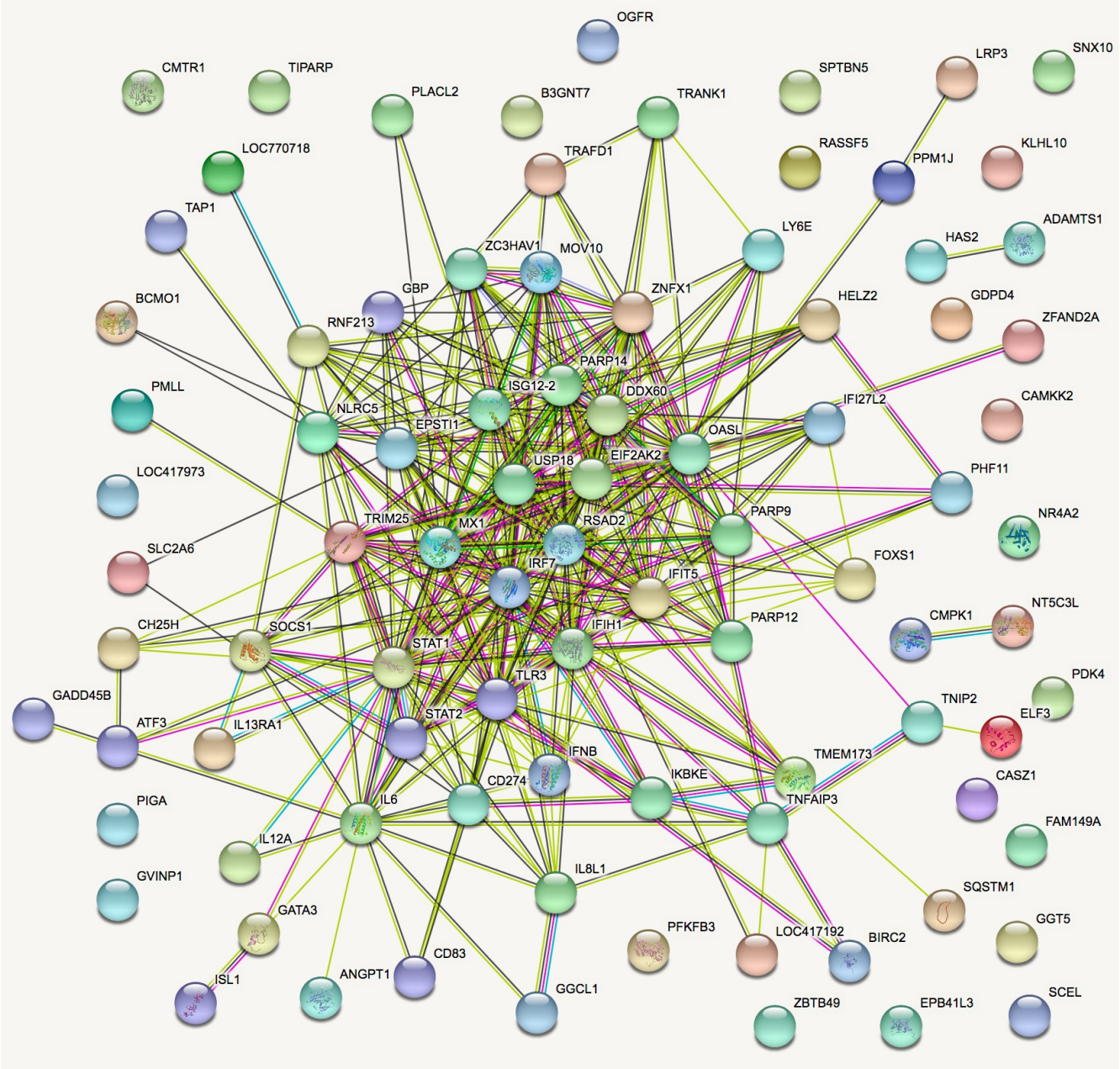

(**E**) Beaudette vs Mock downregulated translation

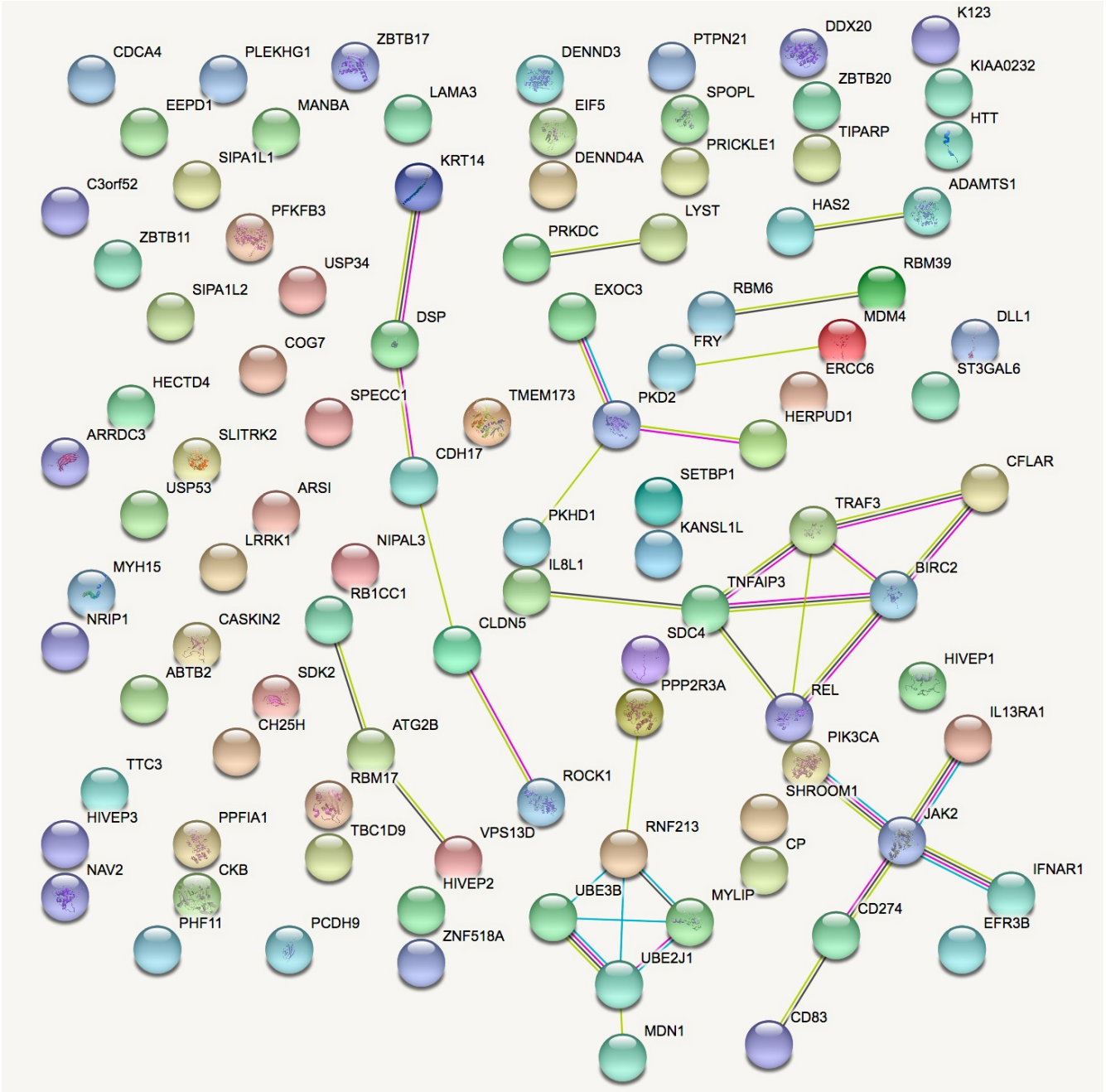

(**F**) M41 vs Mock downregulated translation

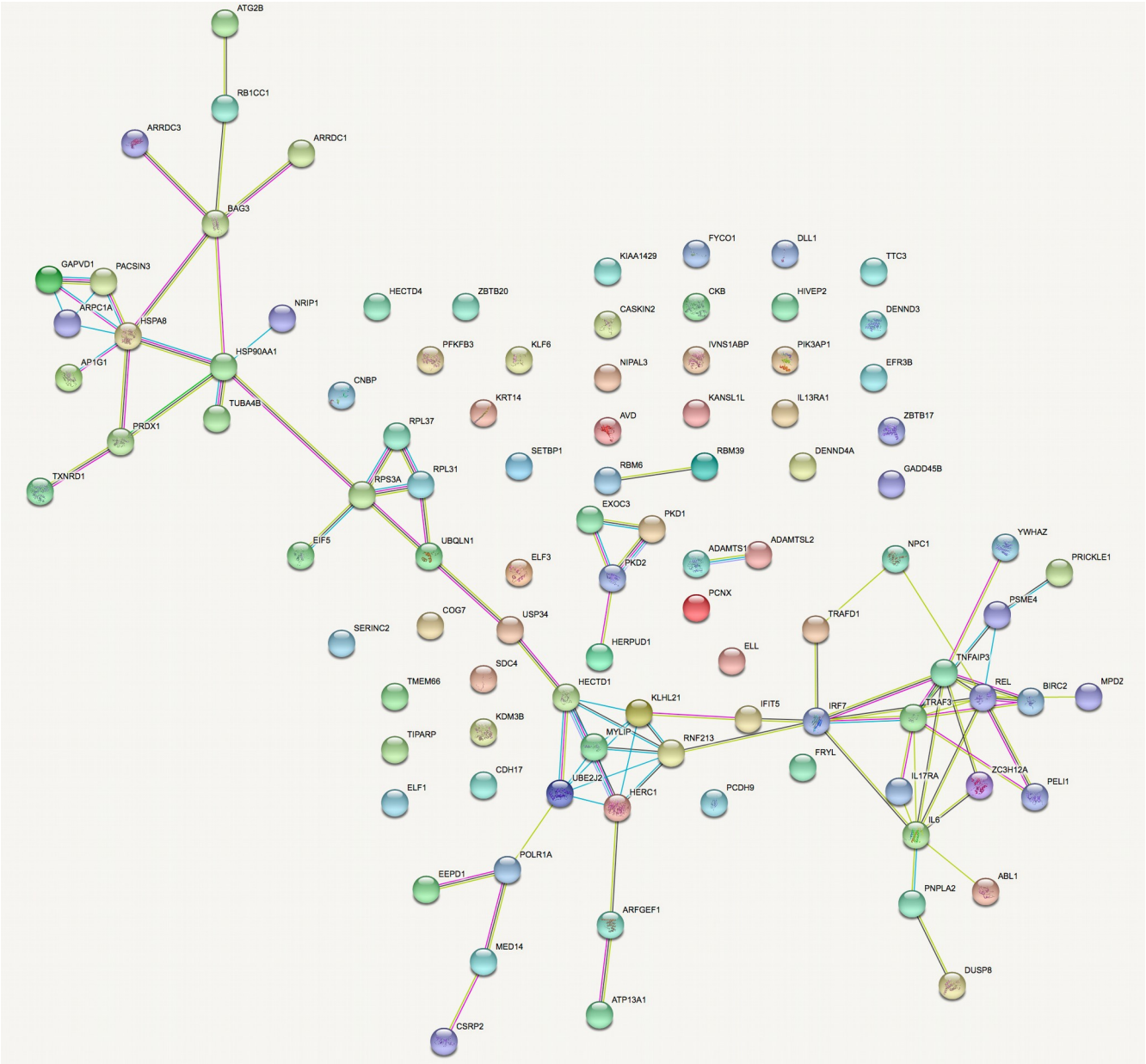

(**G**) Beaudette vs Mock upregulated translation

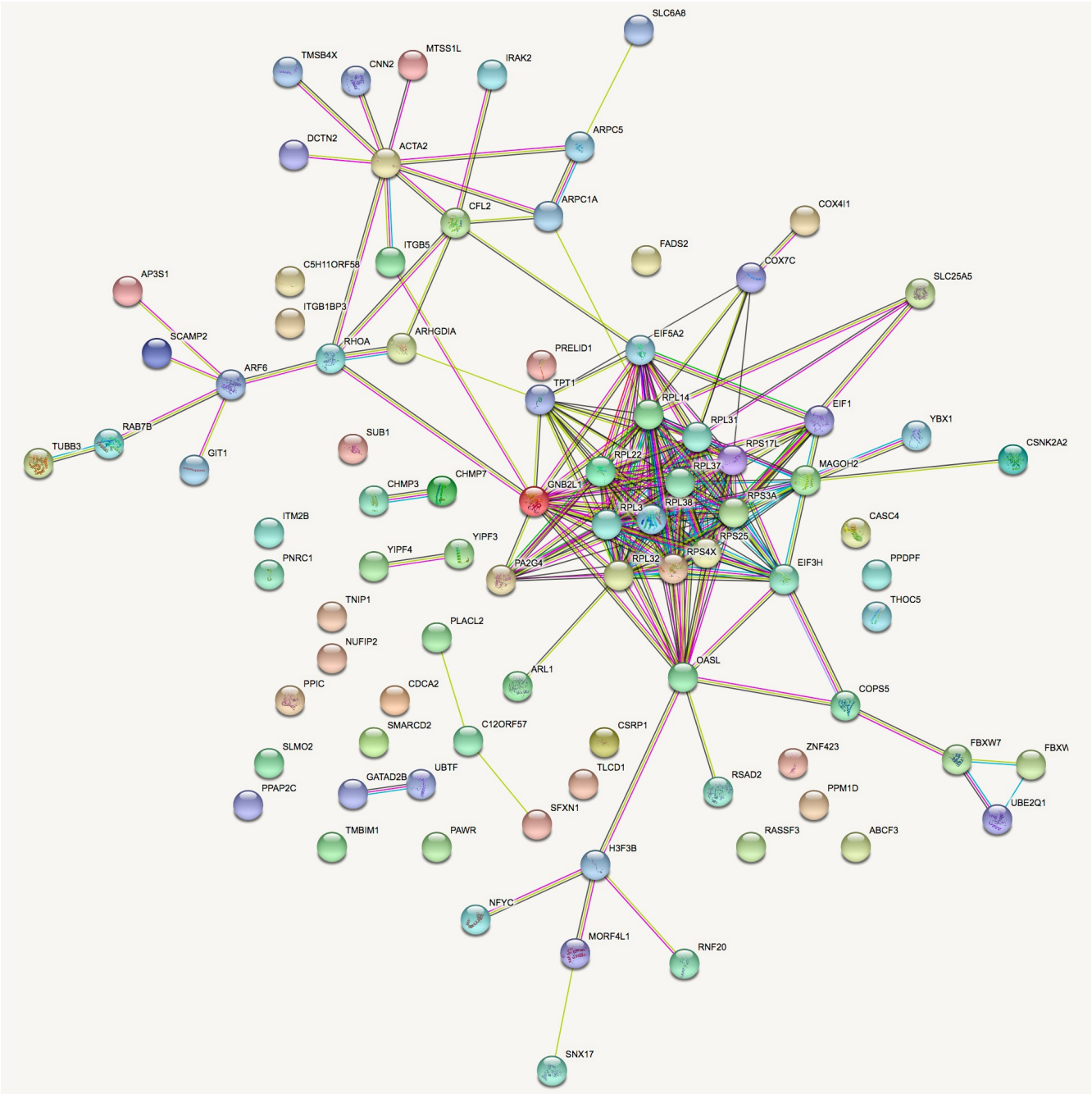

(**H**) M41 vs Mock upregulated translation

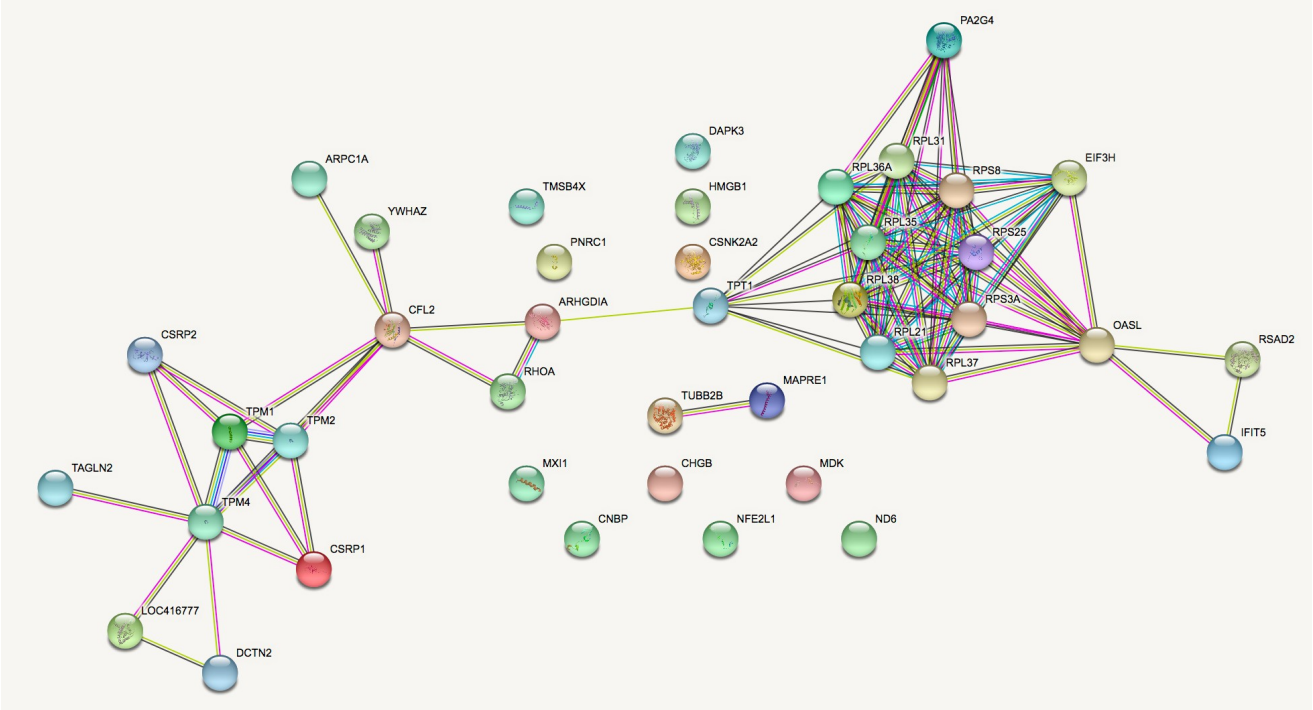

(**I**) M41 vs Beaudette downregulated transcripts

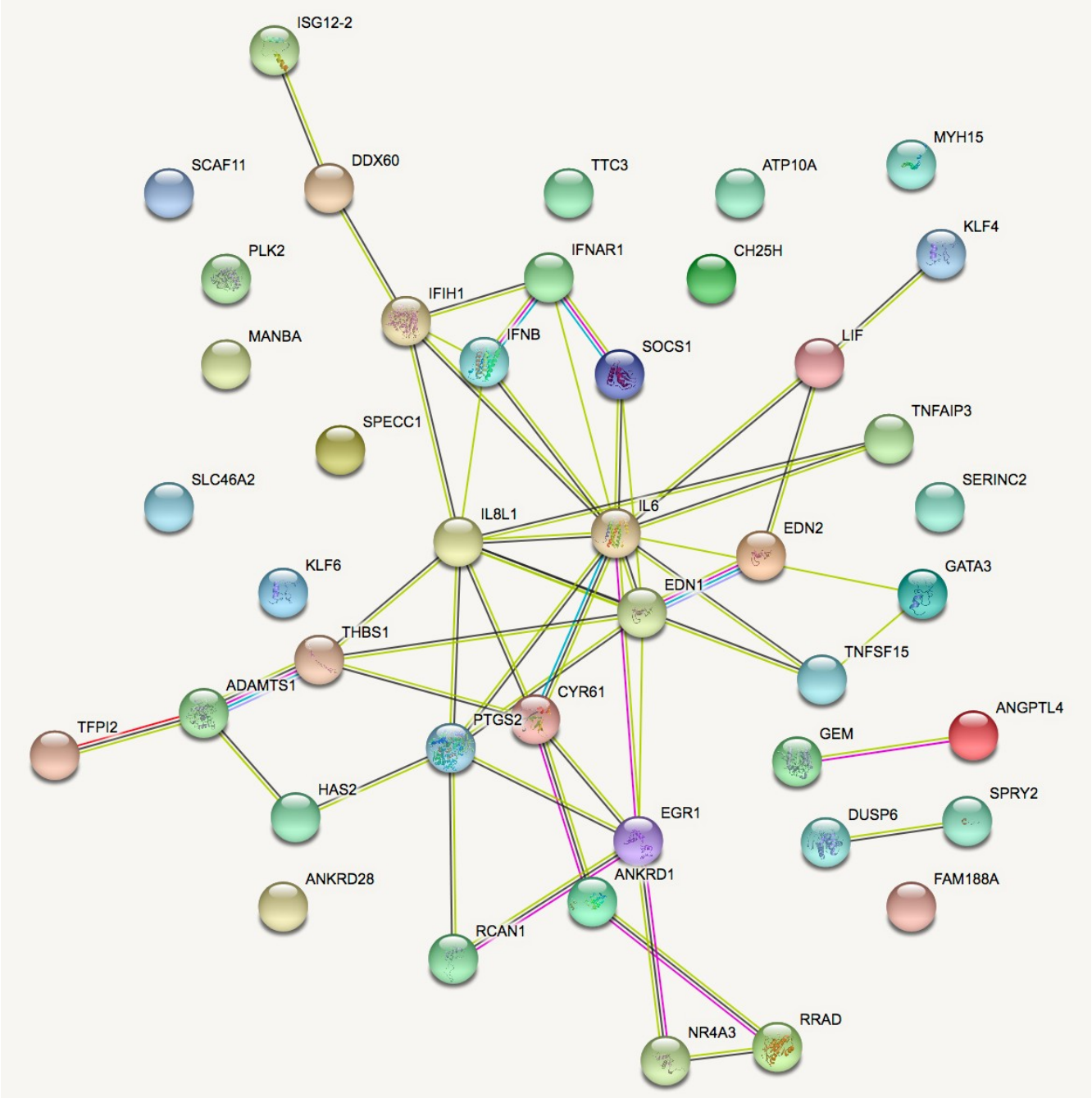

1279
1280
1281
1282
1283
1284
1285
1286